Distinct ribosome states trigger diverse mRNA quality control pathways

Anthony J. Veltri[1], Karole N. D'Orazio[1†], Laura N. Lessen[1‡], Raphael Loll-Krippleber[2], Grant W. Brown[2], Rachel Green[1]

1. Department of Molecular Biology and Genetics, Howard Hughes Medical Institute, Johns Hopkins University School of Medicine, Baltimore, Maryland, USA.
2. Department of Biochemistry and Donnelly Centre, University of Toronto, Toronto, Ontario, Canada.

[†]Present affiliation: Department of Cell Biology, Harvard Medical School, Boston, Massachusetts, USA

[‡]Present affiliation: GlaxoSmithKline, Rockville, Maryland, USA

Abstract

Key protein adapters couple translation to mRNA decay on specific classes of problematic mRNAs in eukaryotes. Slow decoding on non-optimal codons leads to codon-optimality-mediated decay (COMD) and prolonged arrest at stall sites leads to no-go decay (NGD). The identities of the decay factors underlying these processes and the mechanisms by which they respond to translational distress remain open areas of investigation. We use carefully-designed reporter mRNAs to perform genetic screens and functional assays in *S. cerevisiae*. We characterize the roles of Hel2 and Syh1 in coordinating translational repression and mRNA decay on NGD reporter mRNAs, finding that Syh1 acts as the primary link to mRNA decay in NGD. Importantly, we observe that these NGD factors are not involved in the degradation of mRNAs enriched in non-optimal codons. Further, we establish that a key factor previously implicated in COMD, Not5, contributes modestly to the degradation of an NGD-targeted mRNA. Finally, we use ribosome profiling to reveal distinct ribosomal states associated with each reporter mRNA that readily rationalize the contributions of NGD and COMD factors to degradation of these reporters. Taken together, these results provide new mechanistic insight into the role of Syh1 in NGD and define the molecular triggers that determine how distinct pathways target mRNAs for degradation in yeast.

Introduction

Translation of mRNAs to produce proteins is a fundamental cellular process that supports the cell's ability to carry out the basic enzymatic reactions needed for life. To prevent errors that arise during this complex process from compromising cellular metabolism, specialized molecular pathways have evolved to recognize and regulate problematic translation events (D'Orazio and Green 2021; Inada 2017; Yan and Zaher 2019). These mechanisms are coupled to RNA decay pathways that target problematic mRNAs and prevent continuing diversion of ribosomes toward unproductive translation. The set of factors involved in this crucial recognition of problems that arise during translation elongation and the mechanisms by which they exert their downstream effects on mRNA stability remain only partially characterized.

General mRNA decay in yeast is catalyzed primarily by mRNA decapping and 5' to 3' exonucleolytic degradation by Xrn1, while the 3' to 5' exonuclease (the exosome) is thought to play a role only under certain circumstances (Muhlrad, Decker, and Parker 1994). Recent foundational work in yeast, and subsequently in zebrafish and mammals, discovered that mRNA stability is correlated with its codon usage (Presnyak et al. 2015; Mishima and Tomari 2016; Q. Wu et al. 2019): mRNAs enriched in non-optimal codons have short half-lives and are rapidly degraded by the cytoplasmic Ccr4-Not deadenylation complex and the decapping activator Dhh1 (Radhakrishnan et al. 2016; Webster et al. 2018; Sweet, Kovalak, and Coller 2012). Recent biochemical and structural evidence supports a model in which suboptimal codons in the ribosomal A site slow down translation elongation, allowing deacylated tRNA to diffuse away from the E site and enabling the critical adaptor protein Not5 to bind. Not5 binding in the vacant ribosomal E sites can recruit the Ccr4-Not complex to promote mRNA deadenylation, decapping, and decay (Buschauer et al. 2020). These observations provide molecular insight into codon-optimality-mediated decay (COMD) and support for the idea that this pathway represents an important determinant of general cellular mRNA half-lives.

In contrast to the normal slowing of translation that occurs transiently as ribosomes decode less optimal codons, the cell also possesses quality-control machinery to resolve more deleterious ribosomal stalls that can arise from chemical damage in the mRNA (truncation, depurination, nucleobase dimers, oxidative damage, etc.), difficult to unwind secondary structure, or incorrect nuclear mRNA processing events (D'Orazio and Green 2021). Adjacent pairs of specific rare codons can mimic these events and induce strong inhibition of translation elongation and associated mRNA decay in *S. cerevisiae* (Gamble et al. 2016). For example, consecutive CGA codons induce terminal stalls and have been routinely included in reporter mRNAs to trigger an mRNA surveillance pathway referred to as no-go decay (NGD) (Tsuboi et al. 2012; Letzring et al. 2013; Tesina et al. 2020). On these problematic mRNAs, ribosomes stall on the CGA codons, leading to ribosomal collisions that promote small-subunit protein ubiquitination by the E3 ligase Hel2 (mammalian ZNF598), ribosomal clearance by the helicase Slh1 and ribosome quality control trigger (RQT) complex (Ikeuchi, Izawa, and Inada 2019), and nascent peptide decay by the ribosome quality control (RQC) complex (Brandman et al. 2012). The accumulation of colliding ribosomes is thought to trigger decapping and Xrn1-mediated mRNA degradation, though the specific molecular players and interactions responsible for triggering this decay remain poorly defined (D'Orazio et al. 2019; Simms et al. 2019). Additionally, under conditions where the ribosome rescue machinery is compromised or overwhelmed, cleavage of reporter mRNAs by the endonuclease Cue2 and Dom34-mediated rescue provides an alternate route for mRNA degradation and ribosome rescue (Doma and Parker 2006; D'Orazio et al. 2019; Glover et al. 2020). NGD, as a "quality control" pathway, is thought to minimize the detrimental effects from damaged or problematic mRNAs in the cell and to reduce the overall impact of proteotoxic stress (Brandman et al. 2012; Ishimura et al. 2014; Martin et al. 2020).

Though NGD and COMD can be triggered by seemingly similar mRNA sequences and converge on Xrn1-mediated exonucleolytic decay of mRNAs (Pelechano, Wei, and Steinmetz 2015), the extent to which these processes overlap in specificity and activity remains unclear, as do their complete sets of accessory

74 factors. Moreover, the molecular states of the ribosome which define and activate these pathways have
75 not been systematically compared. In this study, we address these questions through genetic screening
76 and functional assays in the yeast *S. cerevisiae*. We use reporter mRNAs designed to trigger NGD or COMD
77 and perform synthetic genetic array (SGA) screens to identify factors critical to these separate mRNA
78 decay pathways. Importantly, we identify a critical role for Syh1 as the primary effector for decay for
79 mRNAs with terminal stalls. We use flow cytometry and northern blotting combined with genetic
80 perturbations to reveal the contributions of other NGD factors and COMD factors to translational
81 repression and decay of the reporter mRNAs. Finally, we use ribosome profiling of NGD and COMD
82 reporters to isolate the activities of the major players in these pathways and connect these activities to
83 the molecular states of elongating ribosomes. These data provide a basis for understanding the unique
84 contributions of each of these pathways to translation-coupled mRNA decay and contextualizes their
85 effects in the larger cellular process of translation surveillance.

86 # Results

87 ## A genetic screen identifies NGD factors in yeast

88 To identify protein factors that contribute to NGD, we developed reporter constructs with well-
89 defined sequence features designed to trigger ribosome stalling and associated quality control. Reporter
90 mRNAs were under the control of the inducible, bidirectional *GAL1-10* promoter and encoded GFP
91 followed by either a fully codon-optimized yeast *HIS3* gene (termed OPT) or *HIS3* interrupted by twelve
92 repeats of the highly non-optimal CGA codon (termed CGA; Figure 1A). This repeat sequence has been
93 shown to trigger NGD in *S. cerevisiae* by causing strong stalling of ribosomal elongation (due to overall
94 low abundance of $tRNA^{Arg(ICG)}$ compounded by inefficient decoding by the I:U wobble interaction) and
95 ensuing ribosome collisions (Letzring, Dean, and Grayhack 2010; Tesina et al. 2020). A viral P2A sequence

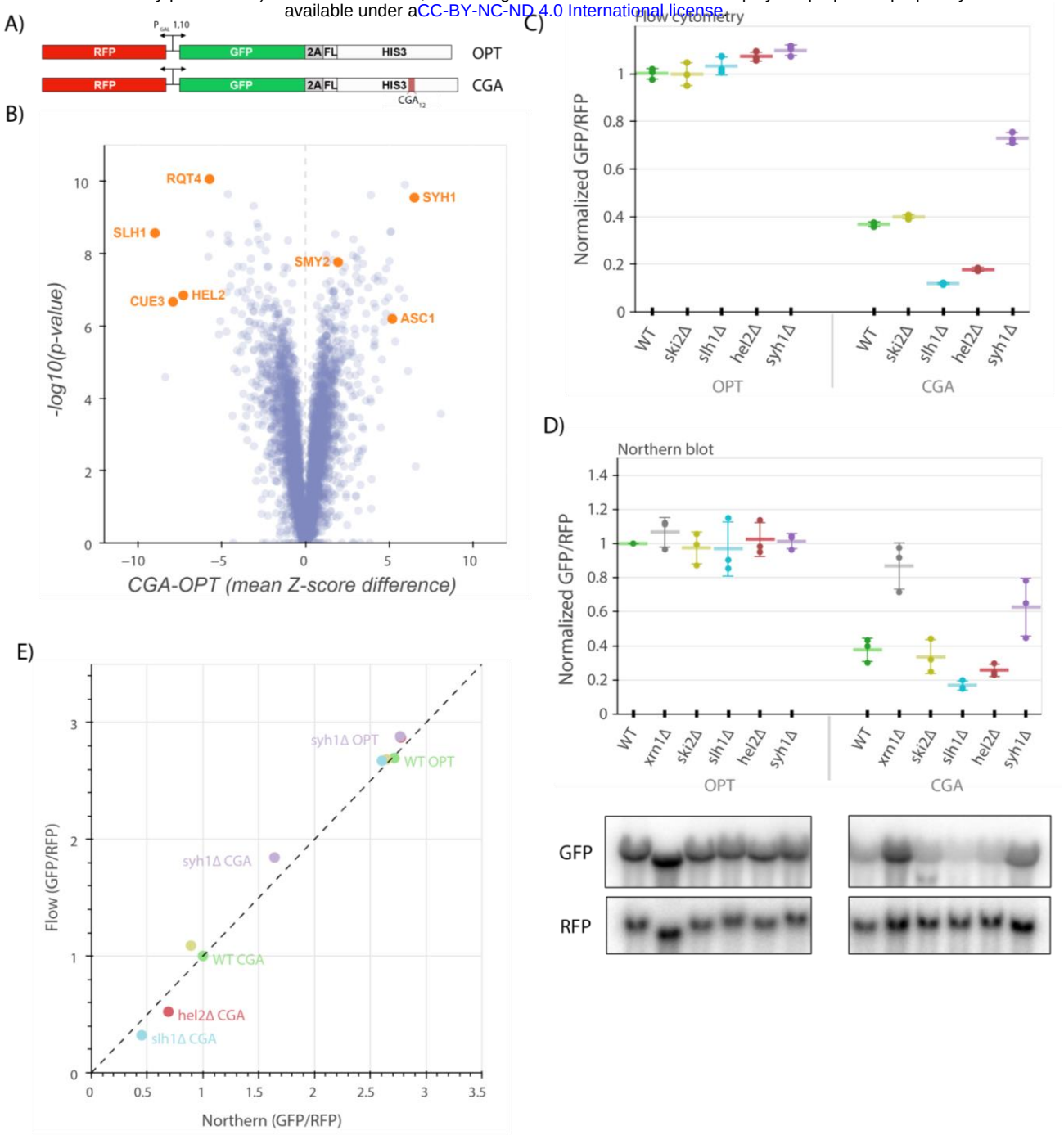

Figure 1: A genetic screen reveals factors that alter levels of an NGD reporter

A) Diagrams of OPT and CGA reporters. Reporters are expressed from a bidirectional *GAL* promoter. GFP is separated from the *HIS3* ORF by a P2A "StopGo" sequence. The CGA reporter contains an insert of twelve CGA codons as a stalling sequence.

B) Volcano plot of data from the R-SGA screen. P-values were calculated from a Fisher's t-test based on per plate GFP/RFP Z-score differences between the CGA and OPT screens. Positive Z-score differences indicate an increase of the CGA reporter relative to the OPT reporter and vice versa. Selected genes are labeled.

C) Flow cytometry analysis of OPT and CGA GFP protein fluorescence reporter levels normalized to RFP fluorescence in several genetic backgrounds. All GFP/RFP levels are normalized to the mean of WT OPT and three replicates are plotted for each strain. Error bars indicate standard deviation.

D) Northern blot analysis of OPT and CGA GFP mRNA reporter levels normalized to RFP mRNA levels quantified by probe hybridization and autoradiography. Three replicates are plotted for each background. All GFP/RFP levels are normalized to the level of WT OPT within each replicate set. Error bars indicate standard deviation. Representative images of the northern blots for one replicate set are shown.

E) The mean reporter levels from panels C and D were normalized and replotted to allow comparison between flow cytometry and northern blot results. All data within each assay were normalized to the mean WT CGA reporter levels.

(Brown and Ryan 2010; Sharma et al. 2012) was inserted between the GFP and *HIS3* open reading frames to decouple GFP levels from the protein decay induced by RQC factors in response to ribosome pausing on CGA codons. Importantly, knockout of *LTN1*, the major E3 ligase responsible for nascent peptide degradation by the RQC complex, did not increase the GFP/RFP ratio for our reporter (Figure S1A), demonstrating that nascent peptide decay does impact the levels of GFP protein. As a result, for this construct, GFP levels serve as a proxy for reporter mRNA levels and translation initiation rates, allowing us to follow these activities in individual cells by flow cytometry. An RFP mRNA is produced from the same *GAL1-10* promoter in the reverse direction, allowing RFP fluorescence to be used to normalize for average transcription and metabolic changes within individual cells.

We performed a Reporter-Synthetic Genetic Array (R-SGA) screen (Fillingham et al. 2009) by introducing the OPT and CGA reporters into the 5377 yeast strains contained in the Yeast Knockout Collection (Giaever et al. 2002). A total of 4222 deletion strains were successfully grown and tested with fluorimetry. We obtained GFP and RFP data for each deletion strain with these two reporters and calculated Z-scores of the GFP/RFP ratio for every strain on a per-plate basis, allowing comparison between the CGA screen and the previously published OPT screen (Figures 1B, S1B) (D'Orazio et al. 2021). To identify genes contributing to NGD, we focused on knockout strains in which normalized CGA reporter levels were significantly increased or decreased relative to our normalized OPT reporter levels (Supplementary Table 1, Figures 1B, S1B). Among the strongest hits from the screen were known NGD factors including *HEL2* and members of the RQT complex (*SLH1*, *CUE3*, and *RQT4*), all of which exhibited substantially decreased GFP reporter fluorescence compared to the wild-type control. This suggests that loss of these factors causes increased decay of the reporter mRNA. Among the strongest hits that increased CGA reporter levels, we identified the ribosomal protein gene *ASC1* and the genes *SYH1* and *SMY2*, homologs of the mammalian NGD factors GIGYF1/2, which we previously reported to impact CGA reporter levels in yeast (Hickey et al. 2020). We also performed a similar R-SGA screen using a reporter

identical to the CGA reporter, except with the CGA_{12} repeat replaced by AAA_{12}; results from this screen showed broad overlap with the CGA reporter screen (Figures S1C-D) as anticipated based on the similar stalling mechanisms of these sequences (Tesina et al. 2020; Koutmou et al. 2015).

Of the CGA reporter strains tested in the original screen, we selected 170 with the strongest increases or decreases in GFP levels (-2 > CGA Z-score > 2 and -2 < OPT Z-score < 2) and individually validated them by flow cytometry to determine which backgrounds affected CGA reporter levels. As in the initial screen, *HEL2*, *SLH1* and *RQT4* as well as *SYH1* and *SMY2* (Supplementary Table 2, Figure S1E) strongly impacted GFP levels, validating our screen results and providing confidence for further mechanistic analysis. A gene set enrichment analysis (GSEA) revealed additional significant hits including genes involved in tRNA modification and protein modification that were not explored further here (Supplementary Table 3, Figure S1F).

Functional assays recapitulate known effects of NGD Factors

To further explore the hits from our genome-wide screen, we deleted genes of interest to verify the observed effects in a clean knockout background and to establish the mechanism of repression for the CGA reporter. We integrated the OPT and CGA reporters at the *ADE2* locus in yeast strains with deletions of *SYH1* and other factors including *HEL2*, *SLH1*, *SKI2* and *XRN1*. While our screen identified two homologs of mammalian GIGYF1/2, our earlier studies had shown that stronger effects were associated with deletion of *SYH1* than with *SMY2* (Hickey et al. 2020), therefore for simplicity, we focused here on the *SYH1* deletion strain. In flow cytometry experiments, we found that the GFP/RFP fluorescence ratios for the OPT reporter were not strongly affected by deletion of HEL2, SLH1, SKI2 or SYH1 (Figure 1C). In the wild-type strain, CGA reporter levels were reduced ~3-fold in comparison to OPT as expected for a reporter subject to active NGD. Consistent with the screen results, CGA reporter levels were further reduced by about 2-fold in the *slh1Δ* and *hel2Δ* strains, while the CGA reporter levels were rescued by ~

1.7-fold in the *syh1Δ* strain (Figure 1C); in contrast, knockout of the *SKI2* gene had no effect on CGA reporter levels.

We next looked directly at mRNA levels in these strains using northern blotting to ask whether GFP levels reflect the mRNA levels. As seen in the flow cytometry assay, OPT mRNA reporter levels were unaltered across all the deletions strains and the CGA mRNA reporter level was reduced relative to the OPT mRNA reporter level in the wild-type strain (Figure 1D). In agreement with the flow cytometry data and previous literature, *ski2Δ* had no effect on CGA reporter levels, whereas *xrn1Δ* strongly rescued reporter levels (D'Orazio et al. 2019; Simms et al. 2019). These results are consistent with the long established importance of Xrn1 in general mRNA decay (Muhlrad, Decker, and Parker 1994) and its critical role in NGD (D'Orazio et al. 2019). Other patterns observed in the flow cytometry data were recapitulated here as well: reporter levels were decreased to a similar extent in the *hel2Δ* and *slh1Δ* strains as in flow cytometry (Figure 1E). And, as revealed by our screen, *syh1Δ* substantially rescued mRNA reporter levels. This focused analysis of protein and RNA reporter levels in these different strains validates results from the initial screen and indicates that the CGA reporter is being strongly regulated by canonical NGD machinery.

Syh1 is the primary NGD factor in yeast

Since screens in this study and our previous work (D'Orazio, et al. 2019) implicated *HEL2*, *CUE2*, and *SLH1* in altering CGA reporter levels, we asked how knockouts of these factors would alter the reporter mRNA levels in an *syh1Δ* strain to get some indication about epistasis. In order to compare more systematically the effects of these knockouts, we turned to a simpler set of reporters expressed from plasmids and containing problematic sequences within the *HIS3* gene but lacking the upstream GFP ORF and the P2A sequence (Figure 2A). The P2A sequence, in particular, has been shown to induce ribosome collisions during translation thus confounding interpretations for certain reporters (C. C.-C. Wu et al.

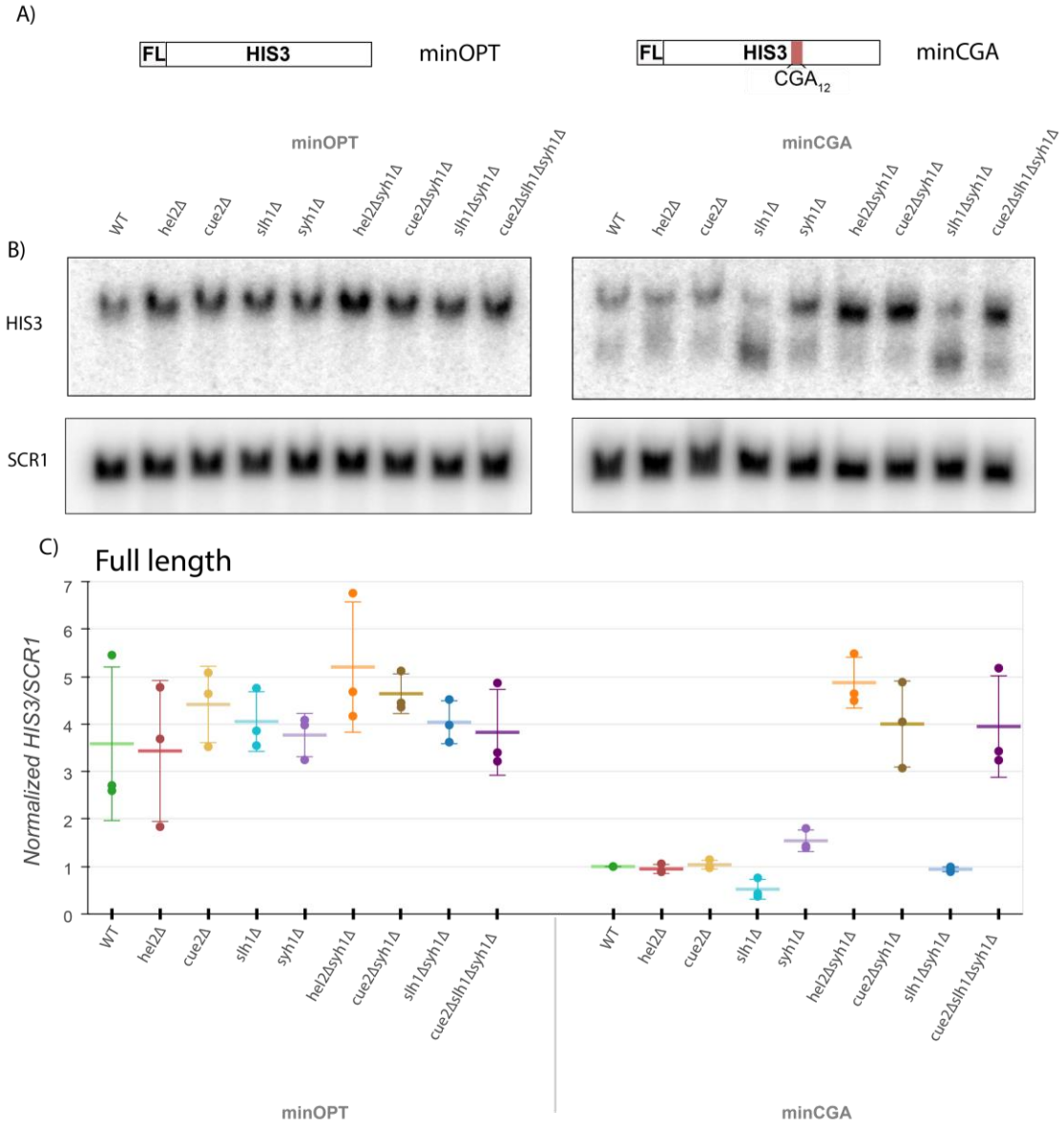

Figure 2: Syh1 is a critical mRNA decay factor for an NGD reporter

A) Diagrams of minOPT and minCGA reporters. Reporters are expressed from a GAL promoter and contain only a FLAG tag and *HIS3* ORF. The minOPT reporter contains a fully-optimized ORF, the minCGA reporter contains a CGA_{12} stalling sequence within the ORF as indicated by red shading.

B) Autoradiograph of northern blot of one representative replicate set of reporter mRNA levels for strains and probes as indicated.

C) Northern blot quantification of minOPT and minCGA *HIS3* mRNA reporter levels normalized to *SCR1* mRNA levels quantified by probe hybridization and autoradiography in yeast strains containing various NGD factor knockouts. Three replicates are plotted. All *HIS3*/*SCR1* RNA levels are normalized to the levels of WT CGA RNA within each replicate set. Error bars indicate standard deviation.

2020). The minOPT reporter is a fully codon optimized, N-terminally FLAG-tagged *HIS3* sequence expressed under a *GAL* promoter, and the minCGA reporter is identical to the minOPT reporter except it includes twelve CGA repeats in the same codon position within *HIS3* as in the GFP-containing CGA reporter used in screening.

To recapitulate our findings with the new minCGA stalling reporter, we used northern blotting to assess the steady-state levels of the reporter mRNA (Figures 2B-C). First, *hel2Δ* does not decrease minCGA reporter levels as observed with the GFP-containing CGA reporter; this discrepancy may arise from effects of the P2A sequence or from differences in levels of expression and thus in ribosome loading. Importantly, although the loss of *CUE2* alone has little effect on the minCGA reporter, the loss of *SLH1* results in a decrease in the amount of full-length mRNA and a corresponding accumulation of a 3' reporter fragment (Figure 2B, *HIS3* probe bottom band; Figures 2C, S2A). This is consistent with our previous studies that established that NGD proceeds through Xrn1 under normal circumstances, whereas the endonuclease Cue2 plays a more important role in the absence of *SLH1* (D'Orazio et al. 2019). In this paradigm, Cue2 acts a failsafe that only cuts mRNAs when stalled ribosomes accumulate when Slh1 is absent or overwhelmed. Finally, here again we observe a modest rescue of reporter levels in the *syh1Δ* strain, consistent with a model where Syh1 recruits Xrn1 and the machinery to mediate decay of the CGA reporter.

To further probe the role of Syh1, we created double knockout strains with *syh1Δ* and other relevant factors and then performed northern blot analysis to follow the levels of the minCGA reporter mRNA. Strikingly, we observe that the *hel2Δsyh1Δ* strain shows a complete rescue of the minCGA mRNA to the levels of the minOPT reporter (Figure 2C). A similar strong rescue was seen with the GFP-containing CGA reporter (Figure S2B). Because Hel2 functions upstream of other NGD factors in its role as an E3 ubiquitin ligase marking colliding ribosomes (Brandman et al. 2012; Saito, Horikawa, and Ito 2015; Matsuo et al. 2017; Sundaramoorthy et al. 2017; Juszkiewicz et al. 2018), the loss of Hel2 has many potential

effects on mRNA decay. We found that the *cue2Δsyh1Δ* strain also showed much higher levels of minCGA reporter, arguing that Cue2 cleavage (which requires Hel2 activity) is the downstream step that degrades mRNA in the absence of Syh1. Further deletion of *SLH1* had little or no additive effect in the *cue2Δsyh1Δ* strain. These results indicate that Syh1 is the major factor contributing to NGD in the absence of *HEL2*, but that Cue2 plays a major compensatory role in decay when Slh1 or Syh1 activity is impaired.

Several recent studies argued that mammalian GIGYF2 is recruited to collided ribosomes by the factor EDF1 (Sinha et al. 2020; Juszkiewicz et al. 2020). *S. cerevisiae* has a homolog of EDF1 known as Mbf1, a protein previously implicated in ribosome-mediated quality control pathways (Hendrick et al. 2001; Wang et al. 2018) that has been shown to interact with collided ribosomes *in vitro* (Sinha et al. 2020; Pochopien et al. 2021). Using tagged Syh1-TAP and Smy2-TAP, we performed affinity purification-mass spectrometry (AP-MS) to search for binding interactions that could help explain the mechanism of action of Syh1/Smy2. While our AP-MS data show strong enrichment of small and large subunit ribosomal proteins, indicating a connection to translation, Mbf1 was not identified as bound to Syh1-TAP or Smy2-TAP (Figure S2C; Supplementary Table 4). Moreover, we find that CGA reporter levels are unaffected in the *mbf1Δ* strain, suggesting that in *S. cerevisiae* this factor is not critical for RNA decay mediated by Syh1 (Figure S2D).

Similarly, we examined CGA reporter expression in yeast strains lacking Eap1, an Syh1-associated translation repressor thought to have a similar mechanism of action to the GIGYF2-associated mammalian protein 4EHP (Sezen, Seedorf, and Schiebel 2009; Cosentino et al. 2000) which is known to work together with GIGYF1/2 to bring about translational repression (Morita et al. 2012; Peter et al. 2019). Again, CGA reporter levels are unaffected in the *eap1Δ* strain relative to WT and in the *eap1Δ* strain relative to *hel2Δeap1Δ* (Figure S2E), meaning that the Syh1-mediated loss in GFP signal occurs independently of Eap1. Additionally, Eap1 was not among the proteins identified in AP-MS (Figure S2C). These data together

suggest that Syh1 recruitment and function in *S. cerevisiae* differs substantially from that observed for GIGYF1/2 in mammalian cells.

COMD does not require canonical NGD factors

Given that the CGA reporter simply contains a stretch of highly non-optimal codons, we wondered whether the same set of factors might similarly regulate ORF sequences containing more widely distributed non-optimal codons. We tested this possibility first by developing a reporter similar to that used for the NGD screen with an N-terminal GFP, an internal P2A sequence, and a downstream *HIS3* gene with an internal stretch of 129 codons synonymously re-coded as non-optimal (NONOPT; Figure 3A). As expected, the NONOPT reporter exhibited substantially diminished GFP levels compared to the OPT reporter and thus provided a starting point for subsequent analysis (Figure 3B).

To identify potential contributing factors to COMD, we performed an R-SGA screen (as above) with this NONOPT reporter (Figure 3C) and again compared these results to our OPT screen results. Strikingly, none of the known NGD factors that we had identified in the previous NGD-CGA screen emerged. These data provide a first indication that NGD mRNAs are regulated very differently from non-optimal mRNAs at the molecular level. Interestingly, factors previously implicated in stabilizing non-optimally coded mRNAs (Webster et al. 2018; Radhakrishnan et al. 2016; Buschauer et al. 2020) were also not among the strains that revealed increases in NONOPT reporter levels (Figure 3C). While some of these strains are not present in the deletion strain collection due to their severe growth phenotype (*dhh1Δ* and *not4/5Δ*), knockouts of several other members of the Ccr4-Not deadenylase complex were present in the screen including *caf40Δ*, *caf130Δ*, and *not3Δ*; among these, NONOPT reporter levels were modestly increased only in the *caf40Δ* strain.

Consistent with the results from the SGA screen, knockouts of the major factors implicated in our analysis of NGD (*hel2Δ* or *syh1*Δ) had no effect on NONOPT reporter expression levels (Figure 3B).

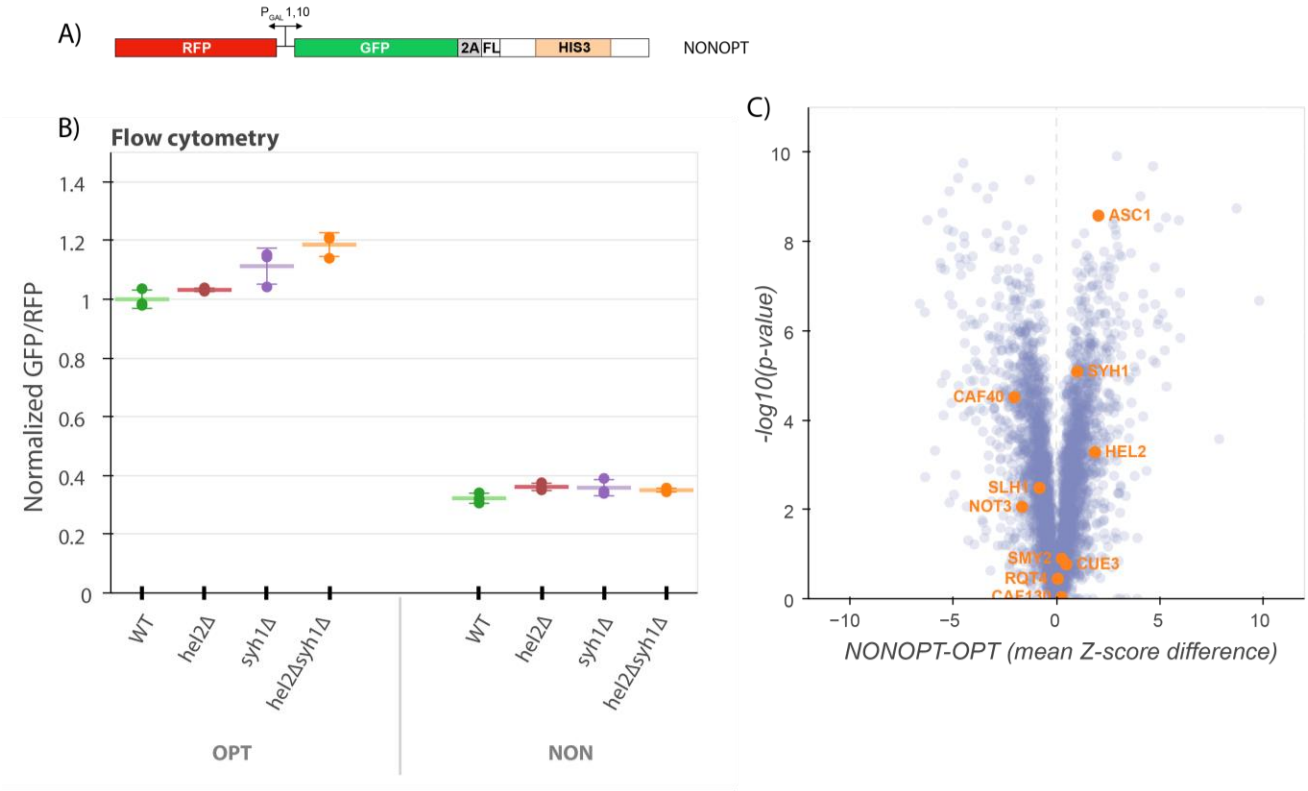

Figure 3: NGD factors do not alter levels of a COMD reporter

A) Diagram of the NONOPT reporter for SGA screening and flow cytometry. Reporter is expressed from a bidirectional *GAL* promoter. GFP is separated from the *HIS3* ORF by a P2A "StopGo" sequence. A portion of the *HIS3* ORF is recoded as synonymous codons with low optimality.

B) Flow cytometry analysis of OPT and NONOPT GFP protein fluorescence reporter levels normalized to RFP fluorescence in yeast strains containing knockouts of *HEL2* and *SYH1* individually and in combination. All GFP/RFP levels are normalized to the mean levels of WT OPT in triplicate. Error bars indicate standard deviation.

C) Volcano plot of the NONOPT R-SGA screen P-values were calculated from a Fisher's t-test based on per plate GFP/RFP Z-score differences between the NONOPT and OPT screens. Positive Z-score differences indicate an increase of the NONOPT reporter relative to the OPT reporter and vice versa. Selected genes are labeled.

Together, these data suggest that there are fundamental differences in recognition by the decay machinery of overall non-optimal coding sequences and more problematic strong translational stalls.

Exploring differences between non-optimal and NGD-triggering mRNAs

In order to compare more systematically the effects of mRNA sequences that trigger NGD or COMD, we turned again to the minOPT and minCGA reporters, with the addition of a third reporter called minNONOPT. This minNONOPT reporter encodes the same *HIS3* ORF recoded with highly non-optimal codons; importantly, there is a short stretch of sequence retained in the minNONOPT reporter that matches the minOPT reporter to allow a common oligonucleotide probe to be used in northern blots (Figure 4A). To evaluate these new reporters, we employed a northern-blot-based transcriptional shutoff assay to measure RNA half-lives as previously reported (Radhakrishnan et al. 2016) in various deletion strains including those implicated above in NGD as well as those previously implicated in COMD.

We first asked whether the half-lives of the minOPT reporter were affected by deletion of the various factors. As anticipated, neither of the factors implicated in regulation of NGD reporters (*HEL2* or *SYH1*) had any discernible effect on the stability of the minOPT reporter mRNA (Figures 4B, S4A-B, Supplementary Table 5). We next determined the effects of the same factors on stability of the minNONOPT mRNA reporter and found that deletion of the NGD factor genes *HEL2* and *SYH1* had no effect while *NOT5* deletion stabilized this mRNA by approximately 11-fold, consistent with earlier reports (Buschauer et al. 2020).

Lastly, we evaluated the effects of the same set of factors on minCGA mRNA stability. There we found that deletion of *HEL2* has no discernible impact on minCGA reporter half-life and deletion of *SYH1* increases half-life 2-fold, while deletion of both factors (*hel2Δsyh1Δ* strain) increases half-life 7-fold, consistent with results from our steady-state northern blots. These results additionally agree with steady-state measurements reported for the screening reporter constructs (Figure S2B). Finally, somewhat

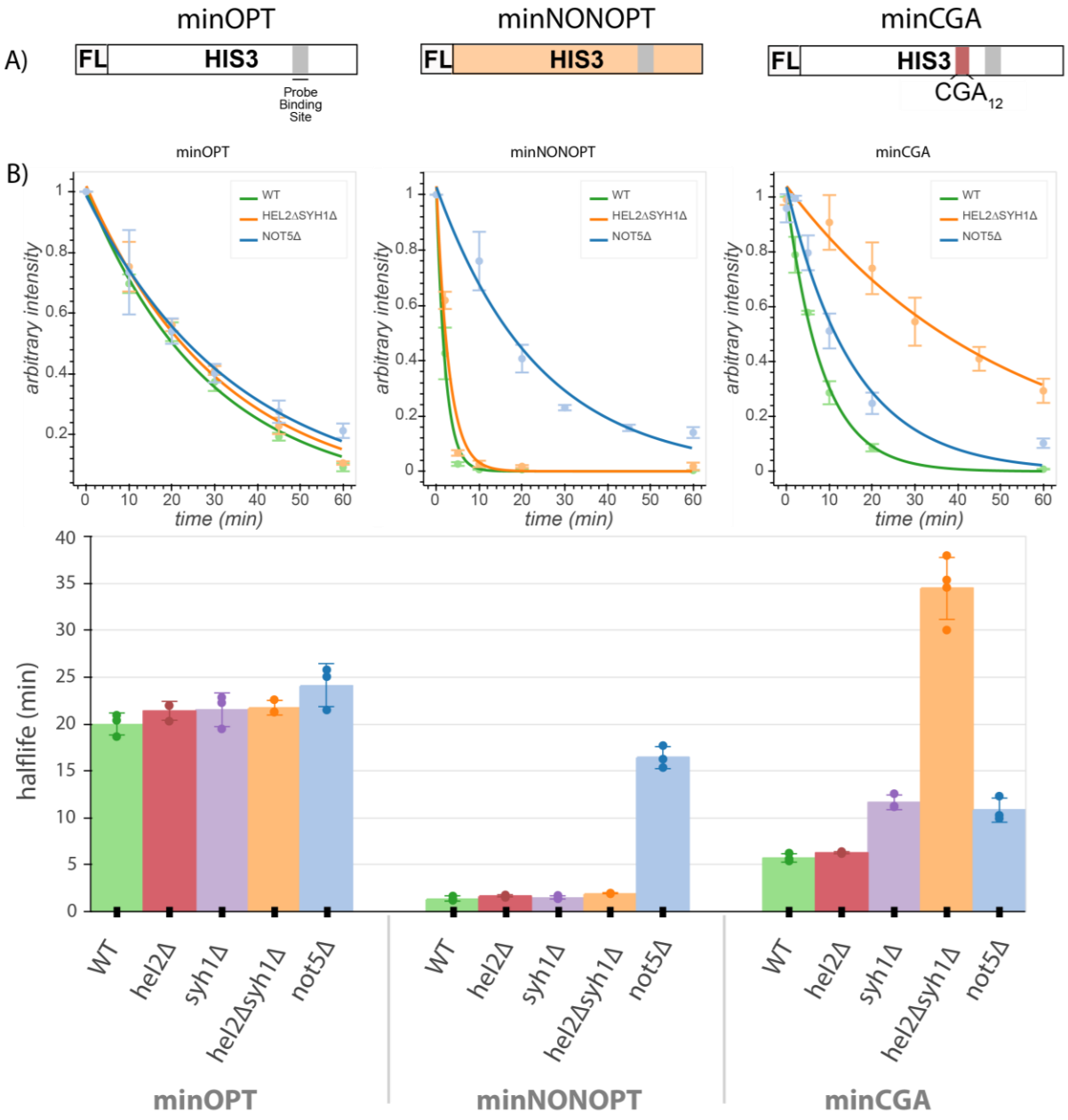

Figure 4: Minimal reporter mRNA half-lives are affected by COMD and NGD factor knockouts

A) Diagram of the minOPT, minCGA, and minNONOPT reporters. Reporters are expressed from a GAL promoter and contain only a FLAG tag and *HIS3* ORF. The minOPT reporter contains a fully-optimized ORF, the minCGA reporter contains a CGA_{12} stalling sequence within the ORF (indicated by the red shaded region), and the minNONOPT reporter contains a *HIS3* ORF fully recoded as synonymous non-optimal codons. All reporters share a common probe binding region for northern blot analysis (shaded in gray).

B) Reporter mRNA half-lives in distinct genetic backgrounds were measured following transcriptional shut down. Reporter mRNA levels were normalized to endogenous *SCR1* levels. Top, reporter mRNA decay curves measured by northern blot analysis after *GAL* promoter shutoff in different genetic backgrounds. A single exponential decay was fit to means of three or four replicates at each timepoint. Bottom, half-lives were calculated for replicates individually by fitting to a single exponential decay and averaged. All error bars indicate standard deviation.

surprisingly, we find that deletion of *NOT5* increases CGA reporter half-life (~2-fold), suggesting features of general non-optimality for this reporter mRNA. Together, these data are broadly consistent with the existence of multiple modes for recognition of troubled elongating ribosomes, each recognized by a distinct set of factors, and leading to decapping and Xrn1-mediated exonucleolytic decay.

Ribosome conformations drive distinct mRNA decay pathways

With the goal of connecting ribosome states to downstream consequences, we next employed ribosome footprint profiling (Ribo-seq) to characterize the positions and conformational states of elongating ribosomes on the minimal reporter mRNAs (Ingolia et al. 2009). To increase the resolution of the approach, both cycloheximide and tigecycline, two specific elongation inhibitors, were added to lysates to capture distinct rotational states of the ribosome during translation represented by two populations of ribosome protected fragment (RPF) lengths centered at approximately 21 and 28 nucleotides (C. C.-C. Wu et al. 2019). The 21-mer population captures ribosomes without A-site tRNAs (waiting to decode) while the 28-mer population captures ribosomes with filled A sites (waiting to translocate). Finally, to further increase the resolution of the study, we separately sequenced single-ribosome (monosome) footprints and those from nuclease-resistant disomes, thought to represent the collided structure that triggers NGD (Guydosh and Green 2014).

We next looked at the distribution of RPFs along our reporter mRNAs. We first see that ribosomes are relatively evenly distributed across the entire ORF in the minOPT reporter for both the 21-mer and 28-mer tracks (Figure 5A). As previously observed for the GFP-containing CGA reporter (Sitron, Park, and Brandman 2017; D'Orazio et al. 2019), we observed that the CGA stall region profoundly disrupts translation of the minCGA ORF. The density of monosome ribosome footprints (both 28- and 21-mers) downstream of the CGA stall is greatly reduced compared to the upstream region on this reporter, indicating that the CGA repeat region comprises a significant translational block (Figure 5A, center; Figure

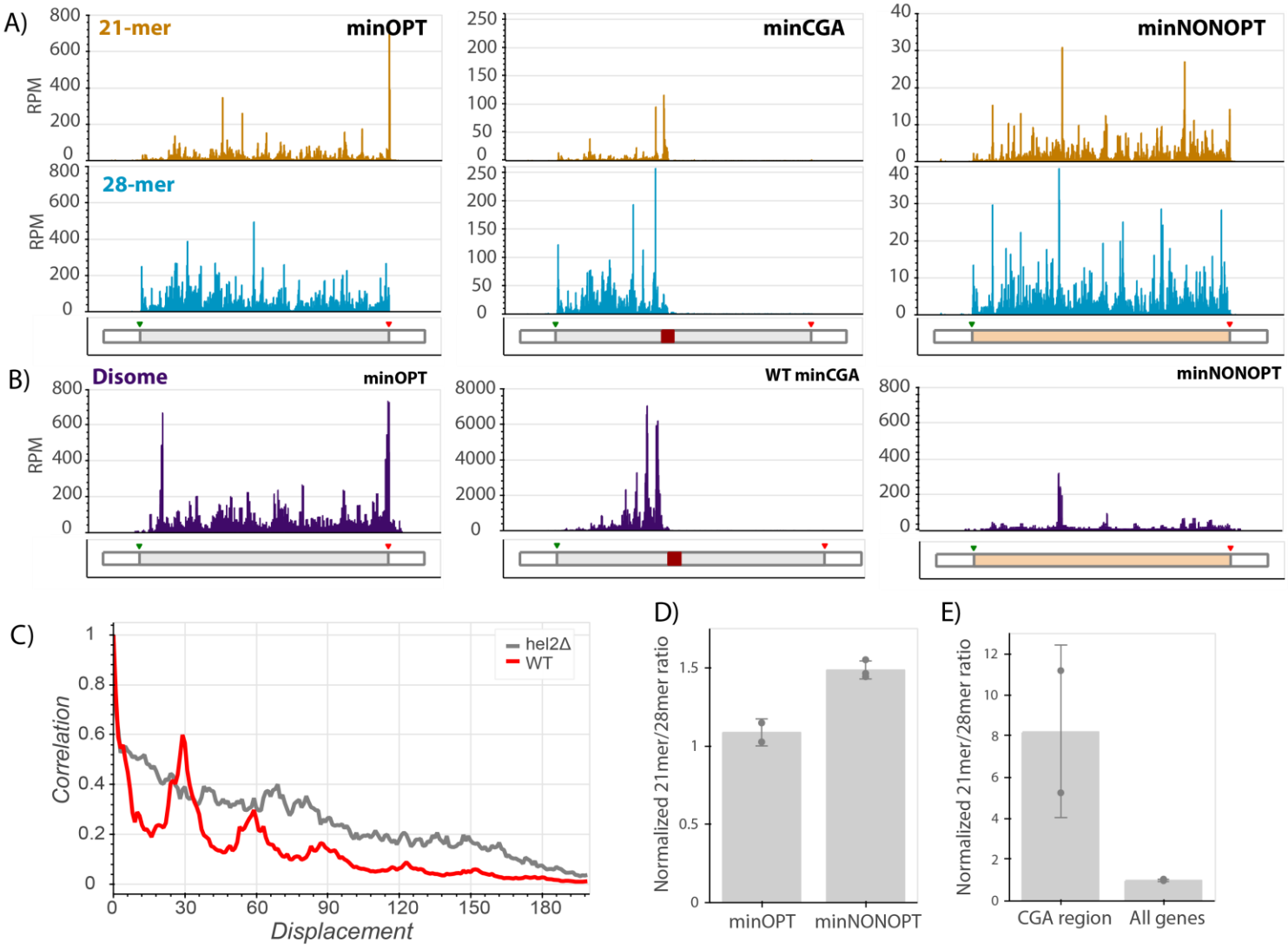

Figure 5: Ribosome profiling reveals translational states that trigger NGD and COMD

A) Gene diagrams show reads per million (RPM) at every position of the indicated reporters: minOPT (left), minCGA (center), minNONOPT (right). Top, 21-mer reads are plotted using read lengths 19-26 inclusive. Bottom, 28-mer reads are plotted using read lengths 27-36 inclusive. Beneath each plot, diagrams of the indicated reporter show the locations of important features.

B) Read RPMs from disome footprint profiling are shown for each position of the minOPT (top) and minNONOPT (bottom) reporters.

C) Autocorrelation of the disome footprint RPMs for WT minCGA and *hel2Δ* minCGA samples.

D) Normalized 21-mer to 28-mer ratios of two replicates for the minOPT and minNONOPT reporters. Ratios exclude regions near the start and end of the ORF and the common probe binding region and are normalized to the 21-mer to 28-mer ratio of all genes to control for differences in digestion efficiency between libraries.

E) Normalized 21-mer to 28-mer ratios of two replicates for multiply aligned reads within the CGA region of the minCGA reporter. Ratios are normalized to the average of 21-mer to 28-mer ratios for all genes.

S5B, top). Importantly, there is a high density of 21-mers near the beginning of the CGA repeat region, consistent with previous reports that decoding of CGA codons is slow. Additionally, 21 and 28-mer peaks appear approximately one footprint length upstream of the CGA stall, extending backwards in a repeating pattern approximately every ribosome length as confirmed by autocorrelation analysis (Figure S5A, S5C top row).

Disome profiling also reveals nuclease-resistant collided ribosome footprints accumulating in this region upstream of the CGA codons; and, autocorrelation analysis reveals that the pattern of "stacked" disomes is periodic with peaks at approximately 30 nucleotide intervals (Figure 5B, center; Figure 5C). In this analysis, disome RPM peaks on the minCGA reporter are dramatically increased (~10-fold) relative to the minOPT reporter, indicative of an accumulation of collided ribosomes (compare scales of minOPT and minCGA panels in Figure 5B). These data together suggest that a key signal for the recruitment of Syh1 and the NGD machinery is the collided ribosome.

To further explore a potential ribosomal basis for the activity of NGD factors on stalling reporter levels, we performed ribosome profiling on the minCGA reporter in *hel2Δ* and *syh1Δ* strains. First, as previously observed (Letzring et al. 2013), deletion of *HEL2* increased ribosome read-through past the stall region relative to the wild-type strain (Figure S5B). Additionally, we noted from the disome profiling that the ordered periodicity in footprint distribution that is present in the WT strain is diminished in the *hel2Δ* strain as revealed by an autocorrelation analysis (Figures 5C, S5D). The same diminished periodicity is observed in monosomes in the *hel2Δ* strain, whereas the ribosome periodicity is generally maintained in the *syh1Δ* strain (Figure S5C).

In contrast to the minCGA reporter, the minNONOPT reporter contains non-optimal codons distributed throughout the ORF; accordingly, monosome footprints are relatively evenly distributed across the ORF (Figure 5A, right panel). Disome footprints are distributed across the ORF as well, suggestive of stochastic short-lived collisions where the ribosome density does not accumulate. To allow

306 for accurate comparison, we performed a more detailed analysis of 21-mer/28-mer ratios for the reporter
307 after excluding the identical oligonucleotide probe region for the two reporters as well as regions around
308 the start and stop codons that can be sensitive to library preparation and variable within ribosome
309 profiling data sets (O'Connor, Andreev, and Baranov 2016). Importantly, we normalized these data from
310 the reporter ORF to global ORF 21-mer/28-mer ratios within each dataset to account for differing RNase
311 digestion efficiencies in the library preparations. Our data reveal an increased 21-mer/28-mer ratio for
312 the minNONOPT relative to the minOPT reporter; as 21-mer RPFs report on empty A sites on the
313 elongating ribosomes, these data are consistent with an enrichment of ribosomes collectively undergoing
314 slow decoding of tRNAs during elongation on non-optimal codons (Figure 5D). These data suggest that a
315 key signal for the recruitment of the COMD machinery (including Not5) is the accumulation of slowly
316 decoding ribosomes.

317 Given the abundance of 21-mer RPFs on the minNONOPT reporter and the strong decay activity
318 of Not5 on this reporter, we wondered whether the activity of Not5 to reduce minCGA reporter half-life
319 (Figure 4B) could be similarly explained by accumulation of 21-mer RPFs. Interestingly, a deeper analysis
320 of the distribution of multiply aligned monosome footprint reads *within* the CGA repeat region of the
321 minCGA reporter revealed that the 21mer/28mer read ratio is greatly enriched compared to the ratio on
322 all genes (Figure 5E). We suggest that this preponderance of slow (21mer RPFs) elongating monosomes in
323 the CGA repeat region might explain the partial sensitivity of the NGD reporter to Not5-mediated
324 destabilization. Since Not5 recognizes ribosomes with open A and E sites, it may be able to bind those
325 ribosomes that continue translating within the CGA_{12} region to elicit decay of the reporter.

326 Taken together, these experiments provide compelling data to rationalize the differing responses
327 of our reporters to various gene knockouts. The accumulation of distinct ribosome signals—either
328 nuclease-resistant collided disomes or slowly decoding ribosomes with empty A sites—acts as a strong
329 determinant for which factors will lead to mRNA destabilization; Syh1 and Hel2 respond to the

accumulation of terminally stalled, collided ribosomes, while Not5 responds to slowly decoding ribosomes with open A and E sites.

Discussion

In this study, we use carefully designed reporter mRNAs to study translation-coupled mRNA decay pathways in *S. cerevisiae*. Using R-SGA screening with a reporter mRNA containing iterated CGA codons, we identified and validated a set of genes that contribute to no-go decay (NGD). Subsequent analysis allowed us to compare the mechanisms of the pathways that regulate decay of mRNAs with either highly problematic (NGD) or slowly decoded sequences (COMD). We find that NGD is driven primarily by the actions of the GIGYF1/2-homologous protein Syh1; in contrast, Syh1 has no discernible impact on the stability of non-optimal mRNA sequences. We show that the previously defined COMD factor Not5 contributes modestly to decay of the NGD reporter and very strongly to decay of non-optimally coded mRNAs. Finally, we connect these distinct molecular decay profiles with ribosome states using ribosome profiling, showing that colliding ribosomes (disomes) are the key trigger for Syh1/Hel2 function while slow ribosomes (monosomes with empty A and E sites) are the key trigger for Not5 function.

Our assays using the NGD reporters reveal the interplay between Hel2, its dependent NGD factors, and Syh1 in responding to ribosome collisions. First, we found that deletion of *SYH1* led to modest stabilization of NGD reporter mRNAs and deletion of *CUE2* and *SYH1* together led to very potent stabilization (Figure 2C). In light of previous work, we interpret the mRNA stability data as follows: 1) in the wild-type strain, the NGD reporters are stabilized because colliding ribosomes lead to the recruitment of Syh1 and elicit mRNA destabilization through Xrn1 while Hel2-mediated ubiquitination triggers ribosomal clearance by Slh1; 2) in the *syh1Δ* strain, NGD reporter levels are somewhat rescued because recruitment of Xrn1 is impaired, but Cue2-mediated endonucleolytic decay plays a larger role as Slh1 becomes overwhelmed; and 3) in the *hel2Δsyh1Δ* and *cue2Δsyh1Δ* strains, NGD reporters are strongly

353 stabilized because both exonucleolytic NGD through Xrn1 and endonucleolytic NGD through Cue2 are
354 inactivated. This model gives new context to the pathways that respond to elongation stalls; it emphasizes
355 the essentiality of Syh1 for Xrn1-mediated NGD and supports our previously discovered mechanism in
356 which the activity of Hel2 primarily triggers RQT-mediated ribosome rescue through Slh1, resorting to
357 Cue2-dependent endonucleolytic cleavage only when other mechanisms to resolve collisions are
358 overwhelmed. The synergistic activities of Syh1-assisted, Xrn1-mediated decay and Hel2-assisted, Cue2-
359 mediated decay form the basis of a robust cellular system for targeting problematic mRNAs for
360 destruction (Figure 6).

361 This interplay was further explored in our Ribo-seq experiments. For the minCGA reporter, we
362 observed an ordered, periodic pattern of monosome and disome footprints upstream of the CGA region
363 in the WT strain, and this pattern was substantially disrupted in the *hel2Δ* strain. Furthermore, we observe
364 a larger proportion of monosome footprints downstream of the CGA region in the *hel2Δ* strains. Given the
365 role of Hel2 in recognizing collided ribosome and promoting clearance by RQT, we interpret these data to
366 mean that the activity of Hel2 on collided ribosomes stabilizes the structure and triggers clearance by Slh1
367 (Meydan and Guydosh 2020), thus preventing ribosome build-up in the downstream region. This stands
368 in contrast to the maintenance of wild-type-like periodicity when *SYH1* is knocked out (Figure S5C).

369 The next set of questions focused on how Syh1 is recruited to problematic mRNAs and how it
370 triggers translational repression or mRNA decay. Recent work in mammalian cells investigating the
371 mechanism of recruitment of GIGYF2 to NGD-targeted mRNAs yielded two competing models: one in
372 which ZNF598 (a mammalian *HEL2* homolog) acts to recruit GIGYF2 (Hickey et al. 2020) and one in which
373 EDF1 acts to recruit GIGYF2 (Sinha et al. 2020; Juszkiewicz et al. 2020). We tested both models. First, we
374 observed strong stabilization of the CGA reporter mRNA levels when *SYH1* is deleted in a *hel2Δ*
375 background (comparing *hel2Δ* to *hel2Δsyh1Δ*) thus establishing that Hel2 function is not necessary for
376 Syh1 function in yeast. Second, we observed the same strong repression of CGA reporter mRNA levels in

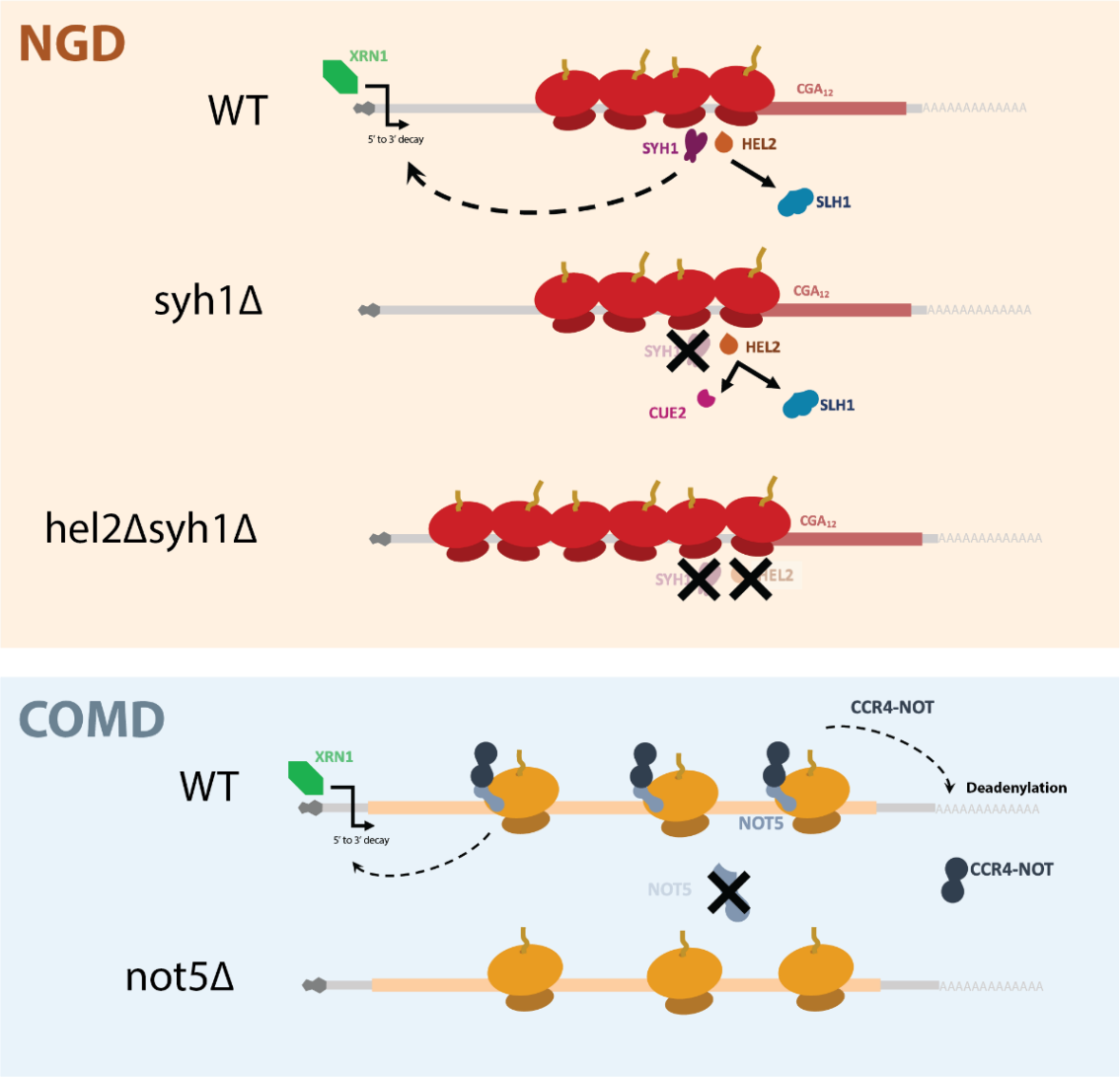

Figure 6: A model for NGD and COMD

In NGD, Syh1 responds to collided ribosomes, connecting severe translational blocks to mRNA decay through decapping and 5' to 3' decay by Xrn1. Loss of Syh1 results in activation of Hel2-dependent endonucleolytic NGD by Cue2. Loss of Syh1 and Hel2 causes increased reporter accumulation by blocking both exonucleolytic and endonucleolytic RNA decay pathways.

In COMD, Not5 senses slow ribosomes on non-optimal codons and recruits the Ccr4-Not complex, causing deadenylation, decapping, and 5' to 3' decay. Loss of Not5 stabilizes non-optimal mRNAs.

a wild-type strain and a knockout of the yeast EDF1 homolog *MBF1* (a result that differs from the rescuing effect of *SYH1* knockout), suggesting that Syh1 function is not dependent on Mbf1. Although Mbf1 binds collided disomes in yeast (Sinha et al. 2020; Pochopien et al. 2021), these data suggest that Mbf1 is not necessary for NGD in yeast. One possibility raised by bioID mass spectrometry (Opitz et al. 2017) is that Syh1 interacts directly with Asc1, a ribosomal protein known to be important for NGD in yeast (Kuroha et al. 2010; Letzring et al. 2013; Brandman et al. 2012), and a top effector of NGD from our genetic screen (Figure 1A). It is possible that Syh1 detects collisions by direct association with collided disomes.

Regarding the downstream effect of Syh1 to activate mRNA decay, we examined a role for the protein Eap1 (a potential functional homolog of the known GIGYF1/2-interacting factor eIF4E2 in mammals), since a direct homolog of eIF4E2 is lacking in yeast. However, deletion of *EAP1* had no discernible effect on our CGA reporter (Figure S2E) suggesting that Eap1 does not function as a bridging factor between Syh1 and Xrn1-mediated mRNA decay. Another candidate effector protein for Syh1 function is Dhh1, whose mammalian homolog DDX6 interacts with GIGYF1/2 to facilitate translational repression (Peter et al. 2019; Weber et al. 2020). In yeast, however, there is only scarce evidence for a Dhh1-Syh1/Smy2 complex (Ergüden 2019) and the conserved DDX6 binding motif of GIGYF1/2 is absent in Syh1/Smy2 (Figure S2F). These data together raise the interesting possibility that Syh1 has a distinct mechanism of regulation in yeast that involves direct signaling of mRNA decay independent of translational repression. We note that the strong mRNA decay phenotype associated with Syh1 function and the NGD reporters in yeast (here and in Hickey, et al. 2020) is distinct from the translational repression phenotype associated with GIGYF2:4E2 function in mammalian systems (Morita et al. 2012; Peter et al. 2019).

Though NGD and COMD both converge on Xrn1-mediated decay of mRNAs, these processes are thought to be triggered distinctly (Radhakrishnan et al. 2016). What has not been clear is whether ribosomes translating highly non-optimal CGA repeats (that efficiently trigger NGD) may also be

recognized by Not5. Conversely, the possibility remained open that highly non-optimal reporter mRNAs cause ribosome collisions that activate NGD in addition to COMD.

We observe that the loss of *NOT5* modestly stabilizes the minCGA reporter, suggesting that the non-optimal decay machinery can respond to slow ribosomes even at sites undergoing NGD. For this reporter, accumulated ribosome footprints from within the CGA-repeat region are short (21-mers), reflect ribosomes with unoccupied A sites as they struggle to decode this problematic sequence (D'Orazio et al. 2019). 21-mer RPFs are also enriched in the minNONOPT reporter. These short footprint reads on both reporters represent very slow ribosomes with open A and E sites that are recognized by Not5, leading to recruitment of the Ccr4-Not complex. This observation rationalizes the modest stabilization of the minCGA reporter and the strong stabilization of the minNONOPT reporter in the *not5Δ* strain. In contrast, we saw no half-life increase of the minNONOPT reporter in the *syh1Δ*, *hel2Δ*, or *hel2Δsyh1Δ* strains, arguing that these abundant non-optimal codons do not induce ribosomal collisions that trigger NGD, consistent with a relatively even distribution and low abundance of disome peaks in the ribosome profiling data. These data provide strong evidence that non-optimal sequences are recognized distinctly from NGD promoting sequences.

Our study provides strong evidence for generally non-overlapping targets and mechanisms of NGD and COMD. While the NGD machinery, under the control of Syh1 and Hel2, responds to specific defects in elongation due to stalled and collided ribosomes, the COMD machinery, under the control of Not5, surveys the pool of translating ribosomes for mRNAs on which there is overall inefficient translation. We speculate that the COMD pathway is a general one that regulates overall mRNA stability, independent of ribosome dysfunction, while the NGD pathway evolved to deal with more acute environmental disturbances such as UV or oxidative damage (Yan et al. 2019; C. C.-C. Wu et al. 2020). Future studies will better characterize the molecular mechanisms of these pathways and will provide new foundations for an understanding of the homeostasis of cellular translation and mRNA decay.

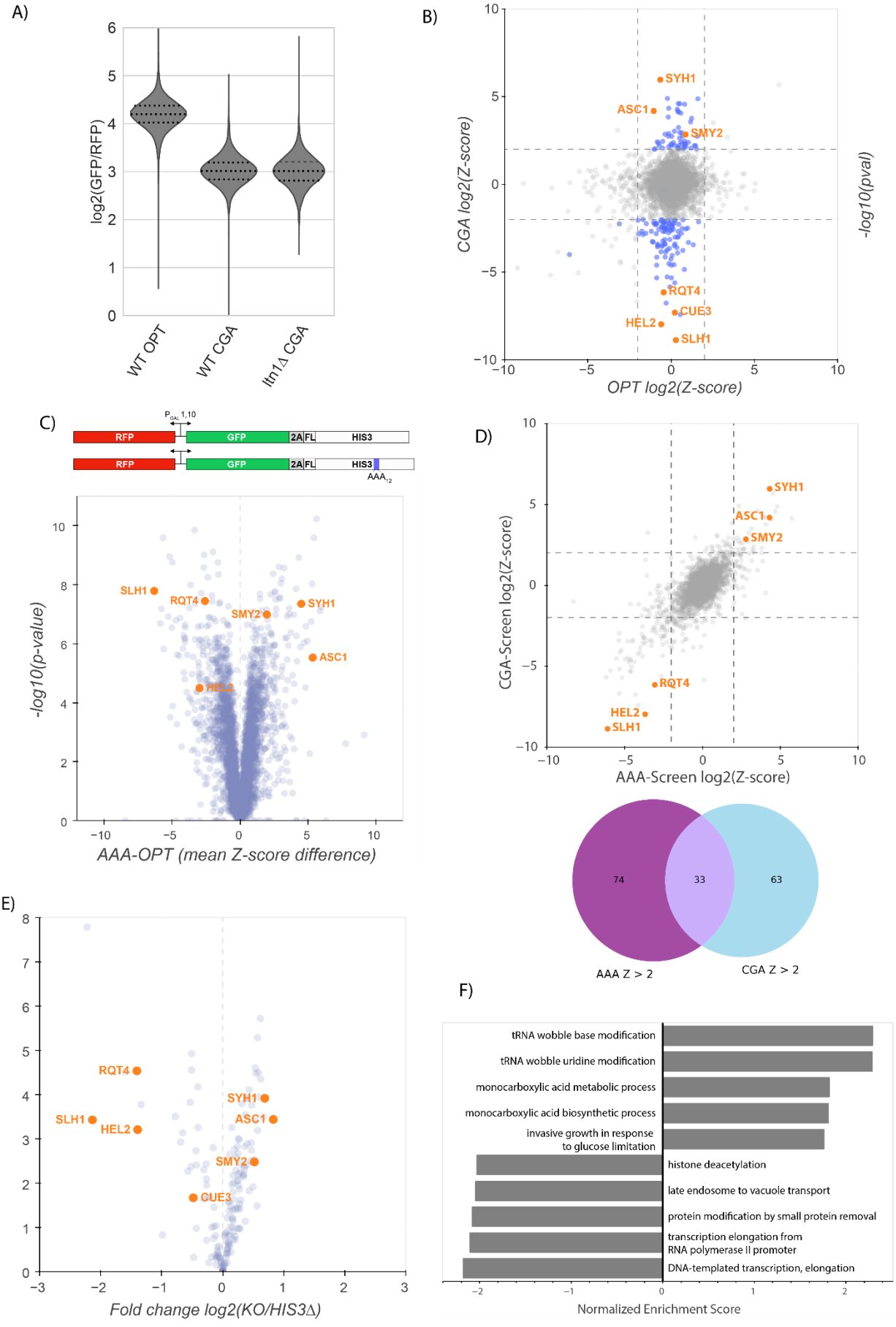

Supplemental Figure 1: Analysis of R-SGA screens and reporters

A) Flow cytometry analysis of OPT and CGA GFP protein fluorescence reporter levels normalized to RFP fluorescence in WT and *ltn1Δ* strains. Distributions represent log2(GFP/RFP) ratios of individual cells. Several known NGD factors are highlighted.
B) Normalized Z-scores based on data from Figure 1B plotted as per-plate z-scores for each gene in the OPT and CGA screens. Genes colored blue (-2 > CGA Z-score > 2 and -2 < OPT Z-score < 2) were selected for follow-up validation.
C) Gene diagrams comparing the OPT and AAA reporters. Similar to the CGA reporter, a stretch of twelve AAA codons were inserted into the HIS3 ORF. Screening data comparing the OPT and AAA screens are plotted as in Figure 1B. Several known NGD factors are highlighted.
D) Normalized Z-scores based on data from Figure S1C from the AAA and CGA screens plotted against each other as in B to emphasize similarity between data from these screens. A Venn diagram shows the overlap between the genes with a Z-score greater than 2 in the CGA and AAA screens.
E) Volcano plot of flow cytometry screen validation with reporters freshly reinserted into knockout collection strains. Fold changes were calculated relative to WT *his3Δ* knockout lines and p-values were obtained from a Fisher's t-test. Several genes are highlighted.
F) Ranked gene-set enrichment analysis for GO terms was performed. Top enriched GO terms from the GO Biological Process annotations were plotted. Positive enrichment scores indicate enrichment among CGA screen hits with positive Z-scores (i.e. knockouts causing increased CGA reporter levels) and vice versa for negative enrichment scores.

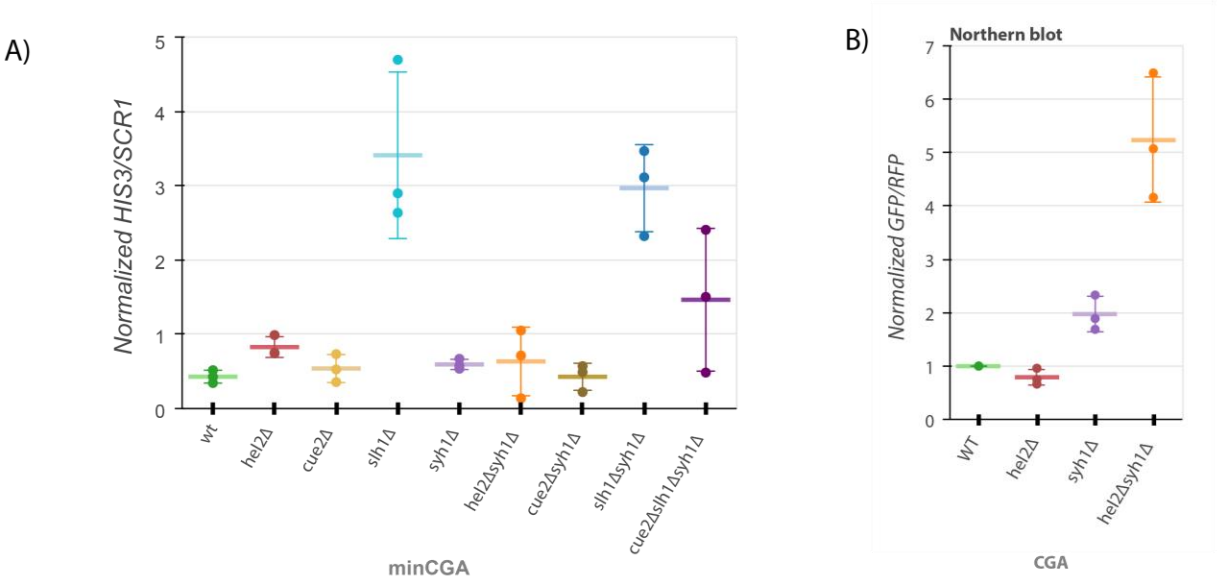

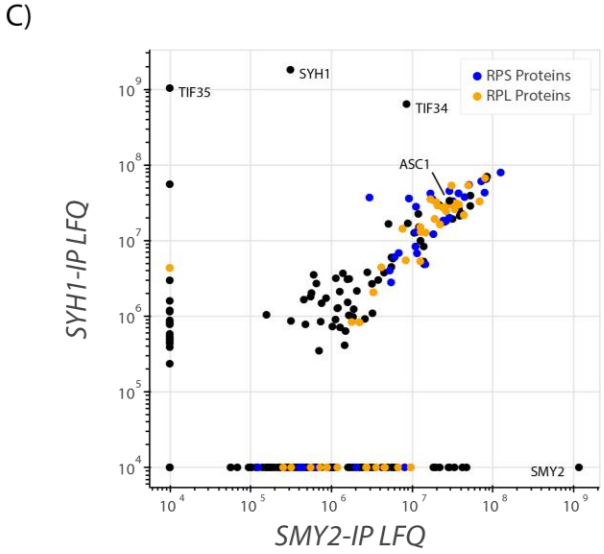

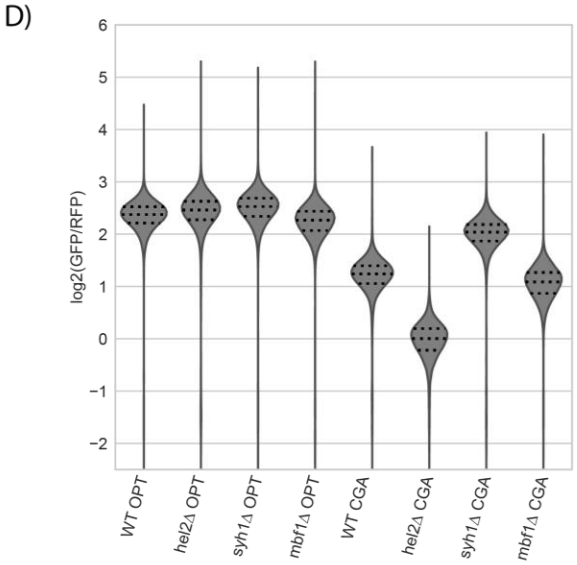

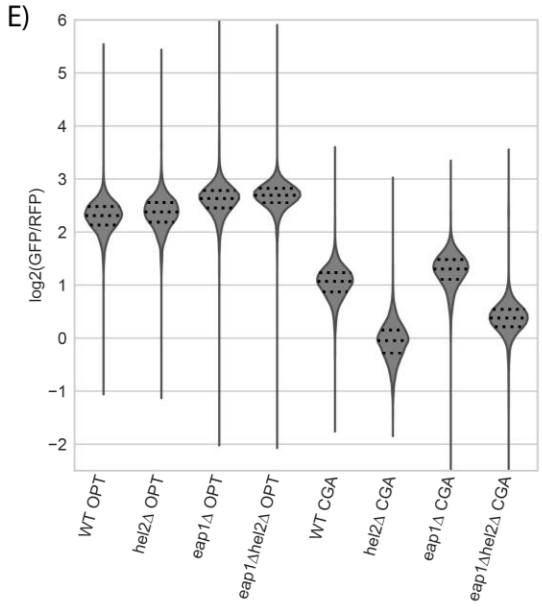

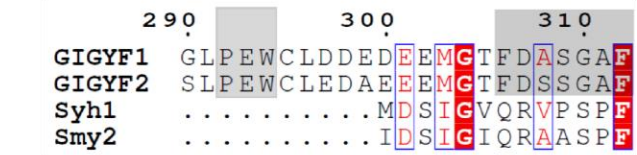

Supplemental Figure 2: Analysis of factors affecting NGD

A) Quantifications of the 3' fragment of the minCGA reporter measured by autoradiographic northern blot as in Figure 2C. Means from three biological replicates are plotted. Data was normalized within each replicate set to the full length WT CGA band as in Figure 2C. Error bars are standard deviation.
B) Quantifications of the full length GFP-containing CGA reporter measured by autoradiographic northern blot as in Figure 1D.
C) Affinity purification-mass spectrometry of Syh1-TAP and Smy2-TAP. LFQ values were calculated using MaxQuant software. Ribosomal (RPS and RPL) proteins are colored orange and blue.
D) Flow cytometry analysis in several strains including *embf1Δ* of OPT and CGA GFP protein fluorescence reporter levels normalized to RFP fluorescence. Distributions represent $\log_2$(GFP/RFP) ratios of individual cells.
E) Flow cytometry analysis in several strains including *eap1Δ* of OPT and CGA GFP protein fluorescence reporter levels normalized to RFP fluorescence. Distributions represent $\log_2$(GFP/RFP) ratios of individual cells.
F) Protein multiple sequence alignment produced by structure-aware alignment with T-Coffee Expresso (Notredame, Higgins, and Heringa 2000). Output diagram was generated by ESPript 3.0 (Robert and Gouet 2014). The GIGYF1/2 conserved binding motif regions from Weber et al. 2020 are indicated by gray shading.

A)

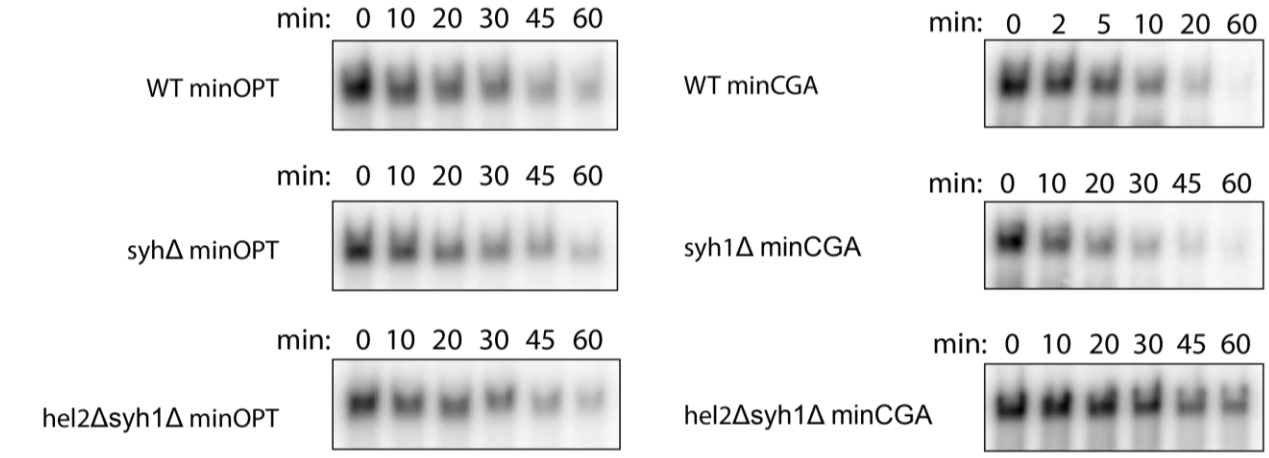

B)

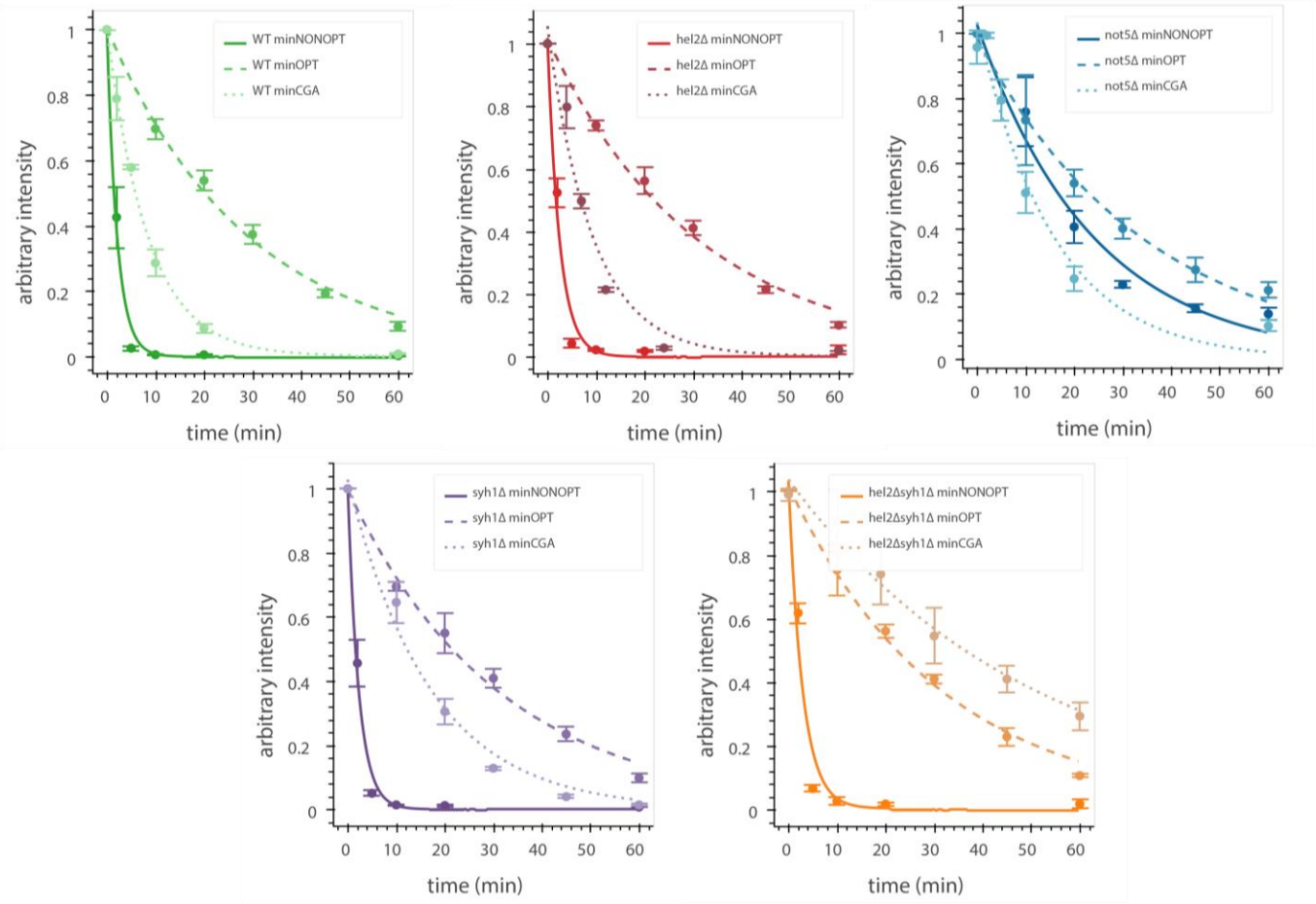

Supplemental Figure 4: Galactose shutoff mRNA decay of reporters in knockout backgrounds

A) Northern blot autoradiography images for reporter mRNAs in galactose shutoff assays in the indicated genetic backgrounds. Representative images are shown.

B) Decay curves for reporters from northern blots are plotted for different backgrounds as in Figure 4B. Reporter mRNA levels were normalized to endogenous *SCR1* levels. Reporter mRNA decay curves measured by northern blot analysis after *GAL* promoter shutoff in different genetic backgrounds. A single exponential decay was fit to means of three or four replicates at each timepoint.

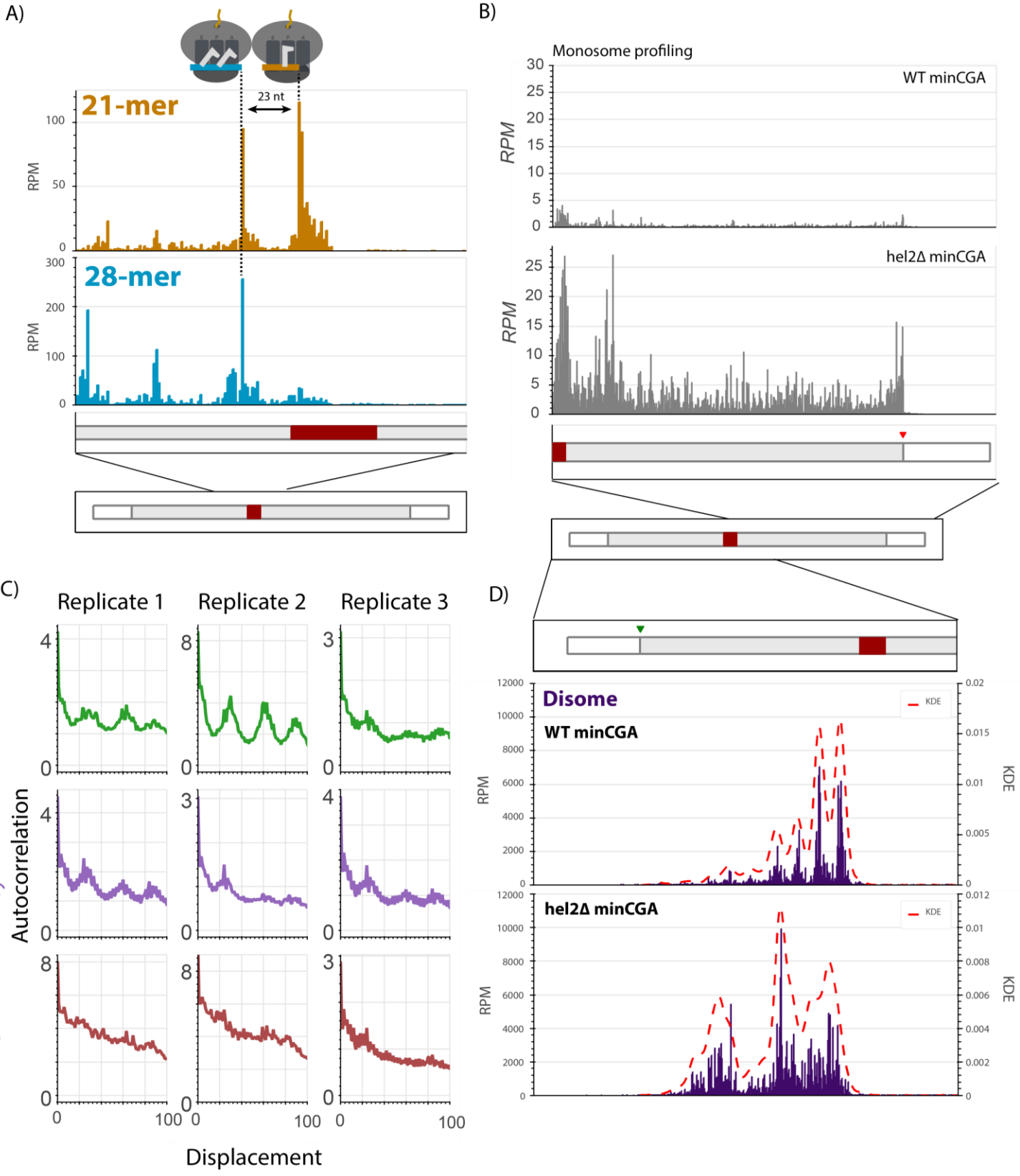

Supplemental Figure 5: Ribosome profiling analysis

A) RPMs for each position of the minCGA reporter replotted from Figure 5A enlarged to show the region around the CGA stall sequence. The leading 21-mer peak and the lagging 28-mer peak are approximately one ribosome length apart.
B) RPMs for each position of the reporter in monosome profiling data for the minCGA reporter replotted from Figure 5A as a combination of all reads compared to the monosome profiling data from the *hel2Δ* strain.
C) Autocorrelation of the footprint RPMs upstream of the stall plotted for three replicates in wild-type, *syh1Δ*, and *hel2Δ* strains.
D) Read RPMs from disome footprint profiling are shown for each position of the minCGA reporter in the WT (top, replotted from Figure 5B) and *hel2Δ* strains. A kernel density estimate (KDE) for each sample was superimposed to emphasize the periodicity of reads in the WT strain that is lost in the *hel2Δ* strain.

Materials and Methods

Reporter cloning & reporter strain generation

Plasmids for OPT (pKD065), NONOPT (pKD064), and CGA (pKD080) reporters were cloned as described in D'Orazio, et al. 2019. To generate stable, genomically integrated strains containing these reporters, 0.5-2 µg of plasmid was digested using StuI to produce an insertion cassette containing the RFP and GFP reporters plus a *MET17* gene for selection, all flanked by homology arms to the endogenous *ADE2* locus. Strains were then transformed by lithium acetate transformation to replace the *ADE2* gene as described below, with the difference of being plated directly onto selective media after transformation rather than a nonselective recovery plate. The minimal reporters minOPT and minNONOPT (plasmids pJC867 and pJC857, respectively) were a generous gift from Jeff Coller and cloned as described in Rhadakrishnan, et al. 2016. The CGA repeat stretch was introduced into the pJC867 plasmid by first isolating the plasmid backbone via digestion with PacI and AscI. Two PCR fragments making up the *HIS3* ORF were generated, one containing the first portion of the *HIS3* ORF and a the CGA repeat region in a primer overhang (primers AV_his3CGAupstr_fwd and AV_his3CGAupstr_rev, see table of oligos), the other containing the downstream *HIS3* sequence and stop codon (primers AV_his3CGAdwnstrm_fw and AV_his3CGAdwnstrm_rv, see table of oligos). Both fragments were amplified off of pJC867 and inserted into the linearized pJC867 backbone using NEB Gibson Assembly Master Mix resulting in pAV_minCGA plasmid. Since these plasmids contained a URA3 selectable marker, reporters were introduced into various backgrounds by transformation of 0.5-1 µg plasmid as described below and all subsequent culture was performed in SC-URA media (plus additives appropriate to experiment) to retain the plasmid.

R-SGA screening

Screening procedure

Screening was performed as described in D'Orazio et al, 2019. Briefly, OPT, CGA, NONOPT, and AAA reporters were inserted into the Yeast Knockout Collection (Giaever et al. 2002) by mating and four replicate colonies were grown for each strain. Incubation times were increased during this process by 50-75% to account for decreased mating efficiency in our query strains. Cells were selected on appropriate media, then plated on 2% GAL/RAF media for expression and analyzed by imaging on a Typhoon FLA9500 imager.

Screen data analysis

Data was analyzed as previously described in D'Orazio et al. 2019 and D'Orazio et al. 2021. OPT screen data used for normalization is the same data previously published in D'Orazio et al. 2021. Briefly, median GFP and RFP values were extracted from colony images using specialized software (Saeed et al. 2003; Wagih et al. 2013) and outliers were excluded (border colonies and those <1500 or >6000 pixels). Average GFP and RFP values from all colonies were then converted to $\log_2$(GFP/RFP) ratios and LOESS normalized on each plate. Z-scores were calculated on a per-plate basis. Z-scores for volcano plots were calculated without prior LOESS normalization.

Screen validation

The 170 Yeast Knockout Collection strains with integrated reporters that showed the greatest change in GFP/RFP for the CGA reporter (-2 > CGA Z-score > 2) and lowest change for the OPT reporter (-2 < OPT Z-score < 2) relative to a *his3*Δ control strain were selected and grown to saturation overnight in YP + 2% galactose + 2% raffinose media in deep-well 96-well plates. Cultures were diluted in triplicate to approximately OD_{600} 0.1 in deep-well 96-well plates and grown to approximately OD_{600} 0.4-0.6. A 10 µL

aliquot of culture was then added to 190 µL PBS and flow cytometry was performed as described below in a Guava EasyCyte HT flow cytometer. P-values were calculated by Fishers T-test.

Yeast strain generation, culture & harvesting

Knockout strain generation

Knockout strains were created using the BY4741 (*MAT***a** *his3Δ1 leu2Δ0 met15Δ0 ura3Δ0*) background as wild-type. DNA fragments containing 40-70 nt homology arms to the gene of interest were amplified by PCR using MX cassette plasmids as template (McCusker 2017) and purified using a Zymo DNA Clean & Concentrator-5 kit. Yeast were then transformed using high-efficiency lithium acetate transformation (Gietz and Schiestl 2007). Briefly, strains to be transformed were grown to saturation at 30 °C overnight in an appropriate medium (typically YPD, YPAD, or SC-Ura), then diluted to OD_{600} 0.2 in 5 mL media. Meanwhile, the transformation mixture was prepared, consisting of 33% PEG 3350, 100 mM LiAc, 0.28 mg/mL boiled salmon sperm DNA, and 1-5 µg PCR product. When cultures reached OD_{600} 0.4-0.6, they were harvested by centrifugation (3000xg, 5 min) and resuspended in the transformation mixture. Transformation mixtures were incubated at 42 °C (or 30 °C for *not5Δ* strains) on a thermomixer for 40-60 minutes, then centrifuged briefly to collect a yeast pellet, discarding the supernatant. Finally, yeast were resuspended in 200 µL water (or media for *not5Δ* strains), plated on an appropriate nonselective agar medium and incubated at 30 °C. Transformants were then streaked to single colonies on a fresh plate, and these colonies were tested for MX cassette insertion by PCR using Phire Plant Direct PCR Master Mix. Confirmed strains were later maintained as patches on selective agar medium.

Growth conditions

Unless noted otherwise, yeast for steady-state reporter expression measurements (by flow cytometry or northern blot) and ribosome profiling were grown to saturation in an appropriate medium lacking glucose and containing 2% galactose and 2% raffinose. Cells were then diluted to OD_{600} 0.1 and

grown to OD_{600} 0.4-0.65 before being harvested according to the requirements of the particular assay to be performed.

Flow cytometry

Cell lines to be analyzed with biological replicates were streaked to single colonies and three individual colonies were selected for outgrowth and analysis. Cells were grown in liquid culture as described above, then 500 µL of cell culture was transferred to a microcentrifuge tube and pelleted by centrifugation. Cells were washed once with PBS and then resuspended in 500 µL PBS. Flow cytometry was carried out using either a Guava EasyCyte or EasyCyte HT instrument, collecting >5000 events. Cellular debris and dead cells were excluded on the basis of forward and side scatter, and geometric means of per-cell GFP/RFP fluorescence distributions were used to calculate GFP/RFP for each replicate (Fig 1, 2A-B, 3) or GFP/RFP ratios were calculated on an individual cell basis for plotting of distributions (Fig S2D-E). For steady state measurements of OPT and CGA reporters in Figs 1C and 2A GFP/RFP ratios were further normalized to the mean of WT OPT or WT CGA replicates, respectively, to place them on a similar scale to northern blotting measurements.

Galactose shutoff RNA half-life assay

Biological replicates of individual cell lines were grown and diluted into 200 mL cultures in SC-URA + 2% Gal + 2% Raf media as described above. The *dhh1Δ* and *not5Δ* strains were typically slow growing and required longer incubations at 30 °C to reach saturation before dilution. When cultures reached OD_{600} 0.4-0.6, they were split into four 50 mL conical tube and pelleted by centrifugation (3000xg, 5 min). Cell pellets were resuspended in 15 mL total prewarmed SC-URA media without added sugar to wash out residual galactose and raffinose and pelleted again by centrifugation in a single 50 mL conical tube. Pellets were resuspended in 10 mL prewarmed SC-URA without added sugar and transferred to a 125 mL beveled flask in a shaking 30 °C incubator. Zero timepoints were taken by removing a 1 mL aliquot of culture,

quickly transferring to a microcentrifuge tube and pelleting cells by a snap spin to 4000xg. Supernatant was decanted and tubes were dropped into liquid nitrogen. To initiate GAL promotor shutoff, 1 mL 40% glucose was added to the 9 mL remaining culture to a final concentration of 4% and a timer was started. Subsequent timepoint samples were taken in a similar manner to the zero timepoint, with the time for each sample recorded at the moment it was dropped into liquid nitrogen. All samples were stored at -80 °C. Downstream RNA extraction and northern blotting proceeded as described below.

Steady state reporter cell harvesting for northern blot

Cells were grown as described above in 10-15 mL. At OD_{600} 0.4-0.6 cultures were pelleted at 4 °C by centrifugation in a 14 mL culture tube, resuspended in 1 mL PBS (or residual growth media), and transferred to a microcentrifuge tube. Cells were pelleted again by centrifugation at 4 °C and supernatant was decanted. Tubes were dropped into liquid nitrogen and stored at -80 °C until RNA extraction.

Northern blotting

RNA extraction

RNA was extracted from frozen cell pellets by hot acid phenol/chloroform extraction. Aliquots of 325 µL acid phenol, pH 4.5 were heated to 65 °C in microcentrifuge tubes on a thermomixer. Cell pellets were retrieved from -80 °C storage and placed on dry ice. Working quickly, individual cell pellets were resuspended in 300-320 µL lysis buffer (8.4 mM EDTA, 60 mM NaOAc pH 5.5, 1.2% SDS) by vortexing just until pellet was fully resuspended. One aliquot of preheated phenol was immediately added to the resuspended pellet and sample was placed onto a thermomixer to minimize time between pellet resuspension and cell lysis. This procedure was repeated for samples being processed in parallel, with each sample shaking at the highest setting on the thermomixer for at least 15 minutes. Tubes were then placed in a dry ice-ethanol bath for ~30 s to help precipitate residual SDS and centrifuged at top speed for

3 minutes. The top aqueous layer was placed in a new tube containing 300 µL room temperature acid phenol. Samples were vortexed several times for a total of 5 minutes, then centrifuged again at max speed for 30 s. The top aqueous layer was transferred to a tube containing 300 mL room temperature chloroform, vortexed several times for a total of 5 minutes, and centrifuged at max speed for 3 minutes. The aqueous phase was then transferred to a tube containing 30 µL 3.5 M NaOAc, pH 5.5. During each step of this process, particular care was taken to avoid transferring any of the organic phase or precipitate at the interface. To each RNA-NaOAc solution, 350 µL of isopropanol was added and mixed well. Tubes were placed on dry ice for at least 30 minutes, or stored at -80 °C overnight. Samples were spun at top speed in a microcentrifuge for 30 minutes and the supernatant was aspirated, taking care not to disturb the RNA pellet. Samples were centrifuged again at max speed for 5 minutes and any remaining supernatant was carefully removed with a 10 µL micropipette. To each RNA pellet, 30 µL of nuclease-free water was added and samples were incubated at 37 °C for 5 minutes on a thermomixer with gentle shaking to facilitate pellet dissolution. Tubes were then moved to ice and pipetted by hand to ensure full pellet resuspension. Finally, RNA concentrations were measured by a nanodrop spectrophotometer and samples were either used immediately for northern blotting or stored at -80 °C for subsequent use.

Gel and RNA preparation

A 1.2% agarose formaldehyde gel was prepared by mixing a final concentration of 1x MOPS electrophoresis buffer, 2.4 g electrophoresis-grade agarose and water to a final volume of 192 mL in a glass 500 mL beaker. This solution was heated in a microwave to boiling and agarose dissolution, mixed, then cooled to approximately 65 °C, placing an insulating material like paper towel beneath to promote even cooling of the solution. Particular care was taken not to allow the agarose to cool further than this before formaldehyde addition, as pieces of unevenly cooled agarose can alter RNA mobility across the gel. When initial cooling was complete, 8 mL 37% formaldehyde and 8 µL ethidium bromide were added and mixed well by swirling. Gel was poured into a mold and allowed to cool fully, then submerged in

formaldehyde gel running buffer (1x MOPS buffer, 1.67% formaldehyde). Meanwhile, RNA samples were prepared by aliquoting an equal mass of total of RNA (typically 10 µg) into microcentrifuge tubes on ice containing an appropriate amount of 5x RNA loading buffer (bromophenol blue, 4 mM EDTA, 2.66% formaldehyde, 20% glycerol, 30% formamide, 4x MOPS buffer).

Gel running and transfer to membrane

RNA samples were boiled at 95 °C for 8 minutes, then cooled to room temp, spun briefly and loaded onto the gel. Gel was run at 100 V for ~2.5 hrs. Gels were imaged on a Typhoon imager to assess RNA quality, then transferred to a Amersham Hybond N+ charged nitrocellulose membrane by a BioRad Model 785 Vacuum Blotter following the manufacturer's instructions for transferring RNA, with the alterations of prewetting the membrane with 10x SSC only and maintaining vacuum between 10-15 inHg. Transfer proceeded for 2 hours. Following transfer, the membrane was carefully removed from the vacuum blotter and placed face up on paper towel for UV crosslinking in a Stratagene UV Stratalinker 2400 on the automatic setting (120 mJ) three times.

Oligonucleotide probe radiolabeling and hybridization

After crosslinking, the membrane was placed in a glass hybridization bottle with the RNA-side facing away from the glass. Approximately 15 mL Sigma Perfecthyb Plus Hybridization Buffer was added to the bottle and it was placed in a hybridization oven to prewarm for 30 min at 42 °C. Meanwhile, the appropriate oligonucleotide probe was enzymatically radiolabeled with the final reaction concentrations 1 µM oligonucleotide probe, 1x NEB T4 PNK buffer, 3-6 µL Perkin Elmer gamma-^{32}P-ATP, 25 units NEB T4 PNK in a 50 µL reaction volume. This reaction was incubated at 37 °C for 1 hr, then the probe was purified using Cytiva Microspin G-50 columns according to the manufacturer's instructions. The entire volume of probe was then added directly to the prewarmed hybridization solution in the hybridization bottle. Membrane and radiolabeled probe were incubated at 42 °C with rotation overnight. The radioactive hybridization solution was discarded and the membrane was washed three times for 20 minutes each

584 with ~15 mL low-stringency wash buffer (0.1% SDS, 2x SSC) at 30 °C. The membrane was placed between
585 transparency film or sheets of plastic wrap and secured into a phosphor storage screen cassette. A blanked
586 phosphor storage screen was exposed to the radioactive membrane long enough to produce adequate
587 exposure (typically overnight) and imaged as described below. To strip hybridized probe off of the
588 membrane, boiling high-stringency wash buffer (0.1% SDS, 0.2x SSC) was poured on the membrane in a
589 hybridization bottle, incubated for 10 minutes at 80 °C, then discarded. The stripping procedure was
590 repeated for a total of two washes, then secondary probing was performed. For experiments with the
591 OPT, CGA, and NONOPT reporters, an oligonucleotide probe for GFP was used as the primary probe and
592 a probe for RFP as the secondary probe. For experiments with minOPT, minCGA, and minNONOPT
593 reporters, a probe for *HIS3* was used as the primary probe and a probe for the endogenous yeast 7S RNA
594 *SCR1* was used as the secondary probe.

595 Phosphor imaging, northern quantification, and half-life calculation

596 Phosphor storage screens were scanned with a typhoon imager and bands were quantified with
597 ImageQuant TL v8.1 software using rolling ball background subtraction. For each blot, the intensity of the
598 primary probe band was normalized to the intensity of the secondary probe band (GFP/RFP for OPT, CGA,
599 and NONOPT; *HIS3*/*SCR1* for minOPT, minCGA, minNONOPT). For galactose shutoff experiments,
600 intensities and timepoints for three or four replicates were fit to a single-exponential decay by least-
601 squares fitting to estimate reporter RNA half-lives. For steady state reporter experiments,
602 reporter/control ratios in Figures 1D and 2B were further normalized to WT OPT and WT CGA within each
603 replicate set, respectively, to correct for any variation between individual blots.

Ribosome profiling

Sample preparation

Ribosome profiling was carried out based on previously published protocols (McGlincy and Ingolia 2017; Guydosh and Green 2014; C. C.-C. Wu et al. 2019).

Culture and ribosome RNA isolation

Cultures were grown to saturation in appropriate media as described above and diluted to OD_{600} 0.1 in 1 L culture. When cells reached OD_{600} 0.4-0.6, cells were harvested by vacuum filtration and pellets were frozen in liquid nitrogen. A portion of each pellet was ground in a SPEX SamplePrep 6870 Freezer/Mill (8 cycles, 10 hz, 1 min run, 1 min cool) with 1 mL pre-frozen lysis buffer (20 mM Tris pH 8, 140 mM KCl, 5 mM $MgCl_2$, 1% Triton X-100, 0.1 mg/mL cycloheximide, 0.1 mg/mL tigecycline) and thawed into 15 mL lysis buffer. Lysates were cleared by centrifugation (5 min, 3000 xg, 4 °C) and supernatants were loaded onto 3 mL sucrose cushion (20 mM Tris pH 8, 150 mM KCl, 5 mM $MgCl_2$, 500 µM DTT, 1 M Sucrose) in a Ti70 ultracentrifuge rotor tube. Samples were centrifuged for 106 minutes at 60,000 RPM, 4 °C to pellet ribosomes. Supernatant was removed, and the ribosome pellet was rinsed once with lysis buffer excluding cycloheximide and tigecycline (drug-free lysis buffer). Pellet was resuspended by pipetting in 1 mL drug-free lysis buffer. RNA concentrations were measured by Qubit RNA High Sensitivity Assay Kit, 350 µg of RNA was added to a microcentrifuge tube, and volume was increased to at least 400 µL with drug-free lysis buffer. 5 µL Ambion RNaseI was added per 400 µL of RNA solution, and samples were incubated at 25 °C in a thermomixer shaking at 500 RPM too digest free RNA. Samples were placed on ice and 10 µL Superase•In RNase inhibitor was added and mixed to stop the RNase digestion. Sucrose gradients were prepared by a Biocomp Gradient Master (15-40% sucrose gradient containing 20 mM Tris pH 8, 150 mM KCl, 5 mM $MgCl_2$, 500 µM DTT) in SW41 ultracentrifuge rotor tubes and RNase reactions were loaded in top of the gradients. Gradients were centrifuged at 40,000 RPM for 2.5 hr at 4 °C. Gradients were

fractionated on a Biocomp Triax gradient fractionator and fractions containing monosomes and disomes were individually pooled and processed in the rest of the downstream protocol. RNA was extracted from samples by SDS-hot phenol/chloroform extraction and isopropanol precipitated with GlycoBlue as co-precipitant.

Ribosome footprint isolation and reverse transcription

RNA pellets were resuspended in 10 mM Tris pH 7.5 and RNA formamide loading dye and run on a 15% TBE-urea gel, taking care to leave empty lanes between samples to minimize cross-contamination. Monosome libraries between 15 and 35 nt (monosomes) or 40 and 70 nt (disomes) were cut out of the gel, frozen, eluted overnight in RNA extraction buffer (300 µM NaOAc pH 5.5, 1 mM EDTA pH 8, 0.25% SDS), and precipitated by isopropanol precipitation. RNA pellets were resuspended in 5 µL dephosphorylation reaction mix (7 mM Tris pH 8, 1x NEB T4 PNK buffer, 10 units Superase•In, 5 units T4 PNK) and incubated at 37 °C for 1 hr. To these reactions, 5 µL of linker ligation mixture was added (38% PEG-8000, 1x NEB T4 ligase buffer, 2 µM oBZ407_preA preadenylated linker, 100 units NEB T4 RNA ligase 2, truncated) and they were further incubated at 37 °C for 3 hrs. Reactions were cleaned up with Zymo Oligo Clean & Concentrator kit and eluted in 10 µL nuclease free water. Samples were supplemented with 1 µL of 10 µM oBZ408 and denatured at 65 °C for 5 mins, then placed on ice. To each sample, 8 µL of reverse transcription reaction was added (2.5x Protoscript II buffer, 12.5 µM DTT, 1.25 mM dNTPs, 20 units Superase•In), samples were mixed, then 1 µL (200 U) Protoscript II reverse transcriptase was added. Samples were incubated 30-60 mins at 50 °C, then RNA templates were hydrolyzed by adding 2.2 µL 1 M NaOH and incubating at 95 °C, 5 min. Samples were again purified with Zymo Oligo Clean & Concentrator kit and eluted in 5 µL nuclease free water.

Ribosomal RNA depletion

A biotinylated subtraction oligo pool from Guydosh & Green, 2014, Cell was prepared as in that publication. To each sample, 1 µL of subtraction oligo pool, 1 µL of 20x SSC, and 2 µL water was added.

Oligos were annealed in a thermocycler, denaturing 90 s at 100 °C, then dropping 0.1 °C/s to 37 °C and incubating 15 mins. MyOne Streptavidin C1 magnetic beads were prepared for RNA binding per the manufacturers protocol and annealed oligo solutions were transferred to the beads. Solutions were incubated for 15 mins at 37 °C, beads were pelleted and supernatants were transferred to new tubes. Samples were cleaned up using Zymo Oligo Clean & Concentrator kit and eluted in 6 µL nuclease free water.

Final sequencing library preparation

Loading dye was added to samples, and they were run on a 10% TBE-urea gel. With the aid of marker oligos, appropriate sizes were cut out from the gel for each sample and DNA was extracted from gel slices as before with DNA extraction buffer (300 µM NaOAc pH 5.5, 1 mM EDTA pH 8, 10 mM Tris pH8). DNA was isopropanol precipitated, resuspended in 20 µL circularization reaction mix (7.75 mM Tris pH 8, 1x Epicentre CircLigase buffer, 50 µM ATP, 2.5 mM $MnCl_2$, 50 units CircLigase), incubated at 60 °C for 2 hr and 80 °C for 10 min. Relative cDNA library abundances were tested by qPCR with BioRad iTaq Universal SYBR Green Supermix to identify an appropriate number of PCR amplification cycles for each library. PCR reactions were then performed for the determined number of cycles to introduce sequencing barcodes and amplify libraries (1x Phusion HF buffer, 200 µM dNTPs, 0.5 µM oBZ287 universal forward PCR primer, 1 µM reverse barcode PCR primer, 7.5% v/v cDNA template, 1 unit Phusion polymerase). Samples were mixed with loading dye and loaded on an 8% TBE PAGE gel. Gel was run 60 min, 200 V and each library was cut from the gel, frozen, and extracted from the gel slice as above using DNA gel extraction buffer. Libraries were isopropanol precipitated, resuspended in 6 µL 10 mM Tris pH 8, and assessed for quality and concentration using an Agilent BioAnalyzer 2100 High Sensitivity DNA assay. Libraries were pooled and sequenced at the Johns Hopkins University Genetic Resources Core Facility on an Illumina NovaSeq 6000 instrument.

Data processing

Reads from raw FASTQ files were trimmed and aligned using a custom Python script to run software from the BBtools suite (https://jgi.doe.gov/data-and-tools/bbtools/) and the STAR aligner (https://github.com/alexdobin/STAR). Subsequent analyses were performed by custom Python scripts. Briefly, reads on start codons from all genes in monosome libraries were used to calculate distances from the 5' end of a read to the ribosomal A site (17 nt for monosomes, 50 nt for disomes). Reads per million mapped reads (RPMs) were calculated at each position of the reporter RNAs by dividing the number of A site shifted 5' ends at a given position by the total number of reads mapped to the genome (not including those that mapped to ncRNA). Reads with lengths 19 to 26 nt were considered part of the 21-mer population and reads with lengths 27 to 35 nt were considered part of the 28-mer population. Ratios of 21-mers/28-mers were calculated by dividing read numbers of 21-mers on the reporter (excluding the FLAG tag, five codons upstream of the top codon and the common binding region of the northern blotting probe) by read numbers of 28-mers on the reporter and normalizing to the 21-mer/28-mer ratio for all genes in a sample (Fig 5E). Ratios of 21-mers/28-mers in the CGA region of the minCGA reporter were calculated by re-aligning unaligned reads allowing multimapping (STAR option --outFilterMultimapNmax 999), then excluding any reads outside the CGA region and counting each unique read only once.

Gene set enrichment analysis (GSEA)

Using data from the CGA screen ranked by per-plate Z-score without LOESS normalization, ranked GSEA was performed using the GSEApy library for Python, querying the GO Biological Process annotation ("GSEApy," n.d.; Xie et al. 2021; Subramanian et al. 2005). The top five most enriched terms in each direction were selected for plotting. Full results are available in the supplemental files.

Affinity purification-mass spectrometry (AP-MS)

TAP-tagged Syh1 and Smy2 strains were purchased from Dharmacon and grown as described above. TAP tag purifications were performed as previously published (Amberg, Burke, and Strathern 2006) replacing NP-40 for Triton X-100 and excluding TCA precipitation. Samples were submitted to the Johns Hopkins University Mass Spectrometry and Proteomics Core facility and processed by facility personnel as follows. Samples were reduced with DTT, alkylated with iodoacetamide and FASP digested on a 30 kDa filter with 10 ng/µl trypsin in 25mM TEAB at 37° C overnight. Peptides were step-fractionated by basic reverse phase chromatography on a µ-HLB Oasis plate. Samples were loaded in 0.1% TFA, eluted with 10 mM TEAB containing 5%, 15%, 20%, 25%, or 50% acetonitrile and fractions were dried. Each fraction was reconstituted in 2% acetonitrile and 0.1% formic acid and injected for MS/MS.

Raw data produced by the core facility was analyzed by MaxQuant (Tyanova, Temu, and Cox 2016) searching against the UniProt yeast database and LFQ values for identified proteins were calculated without imputation, combining data from all fractions of each sample.

Multiple Sequence Alignment

Structure-aware multiple sequence alignment for human GIGYF1 (NCBI accession: O75420.2), GIGYF2 (NCBI accession: Q6Y7W6.1), and yeast Syh1 (NCBI accession: NP_015220.1) and Smy2 (NCBI accession: NP_015220.1) was performed by T-Coffee Expresso (Notredame, Higgins, and Heringa 2000). An additional alignment was performed by EMBL-EBI MUSCLE (https://www.ebi.ac.uk/Tools/msa/muscle) to independently verify alignment results. T-Coffee Expresso alignment results were processed with ESPript 3.0 (Robert and Gouet 2014) and output was included as Figure S2F. Regions corresponding to the DDX6 binding motif identified in Weber et al. 2020 were shaded.

References

Amberg, David C., Daniel J. Burke, and Jeffrey N. Strathern. 2006. "Tandem Affinity Protein (TAP) Purification from Yeast." *CSH Protocols* 2006 (1): db.prot4153.

Brandman, Onn, Jacob Stewart-Ornstein, Daisy Wong, Adam Larson, Christopher C. Williams, Gene-Wei Li, Sharleen Zhou, et al. 2012. "A Ribosome-Bound Quality Control Complex Triggers Degradation of Nascent Peptides and Signals Translation Stress." *Cell* 151 (5): 1042–54.

Brown, Jeremy D., and Martin D. Ryan. 2010. "Ribosome 'Skipping': 'Stop-Carry On' or 'StopGo' Translation." *Recoding: Expansion of Decoding Rules Enriches Gene Expression*. https://doi.org/10.1007/978-0-387-89382-2_5.

Buschauer, Robert, Yoshitaka Matsuo, Takato Sugiyama, Ying-Hsin Chen, Najwa Alhusaini, Thomas Sweet, Ken Ikeuchi, et al. 2020. "The Ccr4-Not Complex Monitors the Translating Ribosome for Codon Optimality." *Science (New York, N.Y.)* 368 (6488): eaay6912.

Cosentino, G. P., T. Schmelzle, A. Haghighat, S. B. Helliwell, M. N. Hall, and N. Sonenberg. 2000. "Eap1p, a Novel Eukaryotic Translation Initiation Factor 4E-Associated Protein in Saccharomyces Cerevisiae." *Molecular and Cellular Biology* 20 (13): 4604–13.

Doma, Meenakshi K., and Roy Parker. 2006. "Endonucleolytic Cleavage of Eukaryotic MRNAs with Stalls in Translation Elongation." *Nature* 440 (7083): 561–64.

D'Orazio, Karole N., and Rachel Green. 2021. "Ribosome States Signal RNA Quality Control." *Molecular Cell* 81 (7): 1372–83.

D'Orazio, Karole N., Laura N. Lessen, Anthony J. Veltri, Zachary Neiman, Miguel Pacheco, Raphael Loll-Krippleber, Grant W. Brown, and Rachel Green. 2021. "Genetic Screens Identify Connections between Ribosome Recycling and Nonsense Mediated Decay." *BioRxiv*. https://doi.org/10.1101/2021.08.03.454884.

D'Orazio, Karole N., Colin Chih-Chien Wu, Niladri Sinha, Raphael Loll-Krippleber, Grant W. Brown, and Rachel Green. 2019. "The Endonuclease Cue2 Cleaves MRNAs at Stalled Ribosomes during No Go Decay." *ELife* 8 (June). https://doi.org/10.7554/eLife.49117.

Ergüden, Bengü. 2019. "Dhh1 Is a Member of the SESA Network." *Yeast* 36 (2): 99–105.

Fillingham, Jeffrey, Pinay Kainth, Jean-Philippe Lambert, Harm van Bakel, Kyle Tsui, Lourdes Peña-Castillo, Corey Nislow, et al. 2009. "Two-Color Cell Array Screen Reveals Interdependent Roles for Histone Chaperones and a Chromatin Boundary Regulator in Histone Gene Repression." *Molecular Cell* 35 (3): 340–51.

Gamble, Caitlin E., Christina E. Brule, Kimberly M. Dean, Stanley Fields, and Elizabeth J. Grayhack. 2016. "Adjacent Codons Act in Concert to Modulate Translation Efficiency in Yeast." *Cell* 166 (3): 679–90.

Giaever, Guri, Angela M. Chu, Li Ni, Carla Connelly, Linda Riles, Steeve Véronneau, Sally Dow, et al. 2002. "Functional Profiling of the Saccharomyces Cerevisiae Genome." *Nature* 418 (6896): 387–91.

Gietz, R. Daniel, and Robert H. Schiestl. 2007. "High-Efficiency Yeast Transformation Using the LiAc/SS Carrier DNA/PEG Method." *Nature Protocols* 2 (1): 31–34.

Glover, Marissa L., A. Max Burroughs, Parissa C. Monem, Thea A. Egelhofer, Makena N. Pule, L. Aravind, and Joshua A. Arribere. 2020. "NONU-1 Encodes a Conserved Endonuclease Required for MRNA Translation Surveillance." *Cell Reports* 30 (13): 4321-4331.e4.

"GSEApy." n.d. https://github.com/zqfang/gseapy.

Guydosh, Nicholas R., and Rachel Green. 2014. "Dom34 Rescues Ribosomes in 3' Untranslated Regions." *Cell* 156 (5): 950–62.

761 Hendrick, J. L., P. G. Wilson, I. I. Edelman, M. G. Sandbaken, D. Ursic, and M. R. Culbertson. 2001. "Yeast
762 Frameshift Suppressor Mutations in the Genes Coding for Transcription Factor Mbf1p and
763 Ribosomal Protein S3: Evidence for Autoregulation of S3 Synthesis." *Genetics* 157 (3): 1141–58.
764 Hickey, Kelsey L., Kimberley Dickson, J. Zachery Cogan, Joseph M. Replogle, Michael Schoof, Karole N.
765 D'Orazio, Niladri K. Sinha, et al. 2020. "GIGYF2 and 4EHP Inhibit Translation Initiation of Defective
766 Messenger RNAs to Assist Ribosome-Associated Quality Control." *Molecular Cell* 79 (6): 950-
767 962.e6.
768 Ikeuchi, Ken, Toshiaki Izawa, and Toshifumi Inada. 2019. "Recent Progress on the Molecular Mechanism
769 of Quality Controls Induced by Ribosome Stalling." *Frontiers in Genetics*.
770 https://doi.org/10.3389/fgene.2018.00743.
771 Inada, Toshifumi. 2017. "The Ribosome as a Platform for MRNA and Nascent Polypeptide Quality Control."
772 *Trends in Biochemical Sciences* 42 (1): 5–15.
773 Ingolia, Nicholas T., Sina Ghaemmaghami, John R. S. Newman, and Jonathan S. Weissman. 2009.
774 "Genome-Wide Analysis in Vivo of Translation with Nucleotide Resolution Using Ribosome
775 Profiling." *Science* 324 (5924): 218–23.
776 Ishimura, Ryuta, Gabor Nagy, Ivan Dotu, Huihao Zhou, Xiang-Lei Yang, Paul Schimmel, Satoru Senju,
777 Yasuharu Nishimura, Jeffrey H. Chuang, and Susan L. Ackerman. 2014. "RNA Function. Ribosome
778 Stalling Induced by Mutation of a CNS-Specific TRNA Causes Neurodegeneration." *Science* 345
779 (6195): 455–59.
780 Juszkiewicz, Szymon, Viswanathan Chandrasekaran, Zhewang Lin, Sebastian Kraatz, V. Ramakrishnan, and
781 Ramanujan S. Hegde. 2018. "ZNF598 Is a Quality Control Sensor of Collided Ribosomes."
782 *Molecular Cell* 72 (3): 469-481.e7.
783 Juszkiewicz, Szymon, Greg Slodkowicz, Zhewang Lin, Paula Freire-Pritchett, Sew-Yeu Peak-Chew, and
784 Ramanujan S. Hegde. 2020. "Ribosome Collisions Trigger Cis-Acting Feedback Inhibition of
785 Translation Initiation." *ELife*. https://doi.org/10.7554/elife.60038.
786 Koutmou, Kristin S., Anthony P. Schuller, Julie L. Brunelle, Aditya Radhakrishnan, Sergej Djuranovic, and
787 Rachel Green. 2015. "Ribosomes Slide on Lysine-Encoding Homopolymeric A Stretches." *ELife* 4
788 (February). https://doi.org/10.7554/eLife.05534.
789 Kuroha, Kazushige, Mayuko Akamatsu, Lyudmila Dimitrova, Takehiko Ito, Yuki Kato, Katsuhiko Shirahige,
790 and Toshifumi Inada. 2010. "Receptor for Activated C Kinase 1 Stimulates Nascent Polypeptide-
791 Dependent Translation Arrest." *EMBO Reports* 11 (12): 956–61.
792 Letzring, Daniel P., Kimberly M. Dean, and Elizabeth J. Grayhack. 2010. "Control of Translation Efficiency
793 in Yeast by Codon-Anticodon Interactions." *RNA (New York, N.Y.)* 16 (12): 2516–28.
794 Letzring, Daniel P., Andrew S. Wolf, Christina E. Brule, and Elizabeth J. Grayhack. 2013. "Translation of CGA
795 Codon Repeats in Yeast Involves Quality Control Components and Ribosomal Protein L1." *RNA*
796 *(New York, N.Y.)* 19 (9): 1208–17.
797 Martin, Paige B., Yu Kigoshi-Tansho, Roger B. Sher, Gianina Ravenscroft, Jennifer E. Stauffer, Rajesh
798 Kumar, Ryo Yonashiro, et al. 2020. "NEMF Mutations That Impair Ribosome-Associated Quality
799 Control Are Associated with Neuromuscular Disease." *Nature Communications* 11 (1): 4625.
800 Matsuo, Yoshitaka, Ken Ikeuchi, Yasushi Saeki, Shintaro Iwasaki, Christian Schmidt, Tsuyoshi Udagawa,
801 Fumiya Sato, et al. 2017. "Ubiquitination of Stalled Ribosome Triggers Ribosome-Associated
802 Quality Control." *Nature Communications* 8 (1). https://doi.org/10.1038/s41467-017-00188-1.
803 McCusker, John H. 2017. "Introducing MX Cassettes into Saccharomyces Cerevisiae." *Cold Spring Harbor*
804 *Protocols* 2017 (4): db.prot088104.
805 McGlincy, Nicholas J., and Nicholas T. Ingolia. 2017. "Transcriptome-Wide Measurement of Translation by
806 Ribosome Profiling." *Methods (San Diego, Calif.)* 126 (August): 112–29.
807 Meydan, Sezen, and Nicholas R. Guydosh. 2020. "Disome and Trisome Profiling Reveal Genome-Wide
808 Targets of Ribosome Quality Control." *Molecular Cell* 79 (4): 588-602.e6.

809 Mishima, Yuichiro, and Yukihide Tomari. 2016. “Codon Usage and 3’ UTR Length Determine Maternal
810 MRNA Stability in Zebrafish.” *Molecular Cell* 61 (6): 874–85.
811 Morita, M., L. W. Ler, M. R. Fabian, N. Siddiqui, M. Mullin, V. C. Henderson, T. Alain, et al. 2012. “A Novel
812 4EHP-GIGYF2 Translational Repressor Complex Is Essential for Mammalian Development.”
813 *Molecular and Cellular Biology*. https://doi.org/10.1128/mcb.00455-12.
814 Muhlrad, D., C. J. Decker, and R. Parker. 1994. “Deadenylation of the Unstable MRNA Encoded by the
815 Yeast MFA2 Gene Leads to Decapping Followed by 5’-->3’ Digestion of the Transcript.” *Genes &*
816 *Development* 8 (7): 855–66.
817 Notredame, C., D. G. Higgins, and J. Heringa. 2000. “T-Coffee: A Novel Method for Fast and Accurate
818 Multiple Sequence Alignment.” *Journal of Molecular Biology* 302 (1): 205–17.
819 O’Connor, Patrick B. F., Dmitry E. Andreev, and Pavel V. Baranov. 2016. “Comparative Survey of the
820 Relative Impact of MRNA Features on Local Ribosome Profiling Read Density.” *Nature*
821 *Communications* 7 (October): 12915.
822 Opitz, Nadine, Kerstin Schmitt, Verena Hofer-Pretz, Bettina Neumann, Heike Krebber, Gerhard H. Braus,
823 and Oliver Valerius. 2017. “Capturing the Asc1p/Receptor for Activated C Kinase 1 (RACK1)
824 Microenvironment at the Head Region of the 40S Ribosome with Quantitative BioID in Yeast.”
825 *Molecular & Cellular Proteomics: MCP* 16 (12): 2199–2218.
826 Pelechano, Vicent, Wu Wei, and Lars M. Steinmetz. 2015. “Widespread Co-Translational RNA Decay
827 Reveals Ribosome Dynamics.” *Cell* 161 (6): 1400–1412.
828 Perez-Riverol, Yasset, Attila Csordas, Jingwen Bai, Manuel Bernal-Llinares, Suresh Hewapathirana, Deepti
829 J. Kundu, Avinash Inuganti, et al. 2019. “The PRIDE Database and Related Tools and Resources in
830 2019: Improving Support for Quantification Data.” *Nucleic Acids Research* 47 (D1): D442–50.
831 Peter, Daniel, Vincenzo Ruscica, Praveen Bawankar, Ramona Weber, Sigrun Helms, Eugene Valkov, Cátia
832 Igreja, and Elisa Izaurralde. 2019. “Molecular Basis for GIGYF-Me31B Complex Assembly in 4EHP-
833 Mediated Translational Repression.” *Genes & Development* 33 (19–20): 1355–60.
834 Pochopien, Agnieszka A., Bertrand Beckert, Sergo Kasvandik, Otto Berninghausen, Roland Beckmann,
835 Tanel Tenson, and Daniel N. Wilson. 2021. “Structure of Gcn1 Bound to Stalled and Colliding 80S
836 Ribosomes.” *Proceedings of the National Academy of Sciences of the United States of America* 118
837 (14): e2022756118.
838 Presnyak, Vladimir, Najwa Alhusaini, Ying-Hsin Chen, Sophie Martin, Nathan Morris, Nicholas Kline, Sara
839 Olson, et al. 2015. “Codon Optimality Is a Major Determinant of MRNA Stability.” *Cell* 160 (6):
840 1111–24.
841 Radhakrishnan, Aditya, Ying-Hsin Chen, Sophie Martin, Najwa Alhusaini, Rachel Green, and Jeff Coller.
842 2016. “The DEAD-Box Protein Dhh1p Couples MRNA Decay and Translation by Monitoring Codon
843 Optimality.” *Cell* 167 (1): 122-132.e9.
844 Robert, Xavier, and Patrice Gouet. 2014. “Deciphering Key Features in Protein Structures with the New
845 ENDscript Server.” *Nucleic Acids Research* 42 (Web Server issue): W320-4.
846 Saeed, A. I., V. Sharov, J. White, J. Li, W. Liang, N. Bhagabati, J. Braisted, et al. 2003. “TM4: A Free, Open-
847 Source System for Microarray Data Management and Analysis.” *BioTechniques* 34 (2): 374–78.
848 Saito, Kazuki, Wataru Horikawa, and Koichi Ito. 2015. “Inhibiting K63 Polyubiquitination Abolishes No-Go
849 Type Stalled Translation Surveillance in Saccharomyces Cerevisiae.” *PLoS Genetics* 11 (4):
850 e1005197.
851 Sezen, Bengü, Matthias Seedorf, and Elmar Schiebel. 2009. “The SESA Network Links Duplication of the
852 Yeast Centrosome with the Protein Translation Machinery.” *Genes & Development* 23 (13): 1559–
853 70.
854 Sharma, Pamila, Fu Yan, Victoria A. Doronina, Helena Escuin-Ordinas, Martin D. Ryan, and Jeremy D.
855 Brown. 2012. “2A Peptides Provide Distinct Solutions to Driving Stop-Carry on Translational
856 Recoding.” *Nucleic Acids Research* 40 (7): 3143–51.

857 Simms, Carrie L., Liewei L. Yan, Jessica K. Qiu, and Hani S. Zaher. 2019. "Ribosome Collisions Result in +1
858 Frameshifting in the Absence of No-Go Decay." *Cell Reports* 28 (7): 1679-1689.e4.
859 Sinha, Niladri K., Alban Ordureau, Katharina Best, James A. Saba, Boris Zinshteyn, Elayanambi
860 Sundaramoorthy, Amit Fulzele, et al. 2020. "EDF1 Coordinates Cellular Responses to Ribosome
861 Collisions." *ELife* 9 (August). https://doi.org/10.7554/eLife.58828.
862 Sitron, Cole S., Joseph H. Park, and Onn Brandman. 2017. "Asc1, Hel2, and Slh1 Couple Translation Arrest
863 to Nascent Chain Degradation." *RNA* 23 (5): 798–810.
864 Subramanian, Aravind, Pablo Tamayo, Vamsi K. Mootha, Sayan Mukherjee, Benjamin L. Ebert, Michael A.
865 Gillette, Amanda Paulovich, et al. 2005. "Gene Set Enrichment Analysis: A Knowledge-Based
866 Approach for Interpreting Genome-Wide Expression Profiles." *Proceedings of the National*
867 *Academy of Sciences of the United States of America* 102 (43): 15545–50.
868 Sundaramoorthy, Elayanambi, Marilyn Leonard, Raymond Mak, Jeffrey Liao, Amitkumar Fulzele, and Eric
869 J. Bennett. 2017. "ZNF598 and RACK1 Regulate Mammalian Ribosome-Associated Quality Control
870 Function by Mediating Regulatory 40S Ribosomal Ubiquitylation." *Molecular Cell* 65 (4): 751-
871 760.e4.
872 Sweet, Thomas, Carrie Kovalak, and Jeff Coller. 2012. "The DEAD-Box Protein Dhh1 Promotes Decapping
873 by Slowing Ribosome Movement." *PLoS Biology* 10 (6): e1001342.
874 Tesina, Petr, Laura N. Lessen, Robert Buschauer, Jingdong Cheng, Colin Chih-Chien Wu, Otto
875 Berninghausen, Allen R. Buskirk, Thomas Becker, Roland Beckmann, and Rachel Green. 2020.
876 "Molecular Mechanism of Translational Stalling by Inhibitory Codon Combinations and Poly(A)
877 Tracts." *The EMBO Journal* 39 (3): e103365.
878 Tsuboi, Tatsuhisa, Kazushige Kuroha, Kazuhei Kudo, Shiho Makino, Eri Inoue, Isao Kashima, and Toshifumi
879 Inada. 2012. "Dom34:Hbs1 Plays a General Role in Quality-Control Systems by Dissociation of a
880 Stalled Ribosome at the 3' End of Aberrant MRNA." *Molecular Cell* 46 (4): 518–29.
881 Tyanova, Stefka, Tikira Temu, and Juergen Cox. 2016. "The MaxQuant Computational Platform for Mass
882 Spectrometry-Based Shotgun Proteomics." *Nature Protocols* 11 (12): 2301–19.
883 Wagih, Omar, Matej Usaj, Anastasia Baryshnikova, Benjamin VanderSluis, Elena Kuzmin, Michael
884 Costanzo, Chad L. Myers, Brenda J. Andrews, Charles M. Boone, and Leopold Parts. 2013.
885 "SGAtools: One-Stop Analysis and Visualization of Array-Based Genetic Interaction Screens."
886 *Nucleic Acids Research* 41 (Web Server issue): W591-6.
887 Wang, Jiyu, Jie Zhou, Qidi Yang, and Elizabeth J. Grayhack. 2018. "Multi-Protein Bridging Factor 1(Mbf1),
888 Rps3 and Asc1 Prevent Stalled Ribosomes from Frameshifting." *ELife* 7 (November).
889 https://doi.org/10.7554/eLife.39637.
890 Weber, Ramona, Min-Yi Chung, Csilla Keskeny, Ulrike Zinnall, Markus Landthaler, Eugene Valkov, Elisa
891 Izaurralde, and Cátia Igreja. 2020. "4EHP and GIGYF1/2 Mediate Translation-Coupled Messenger
892 RNA Decay." *Cell Reports* 33 (2): 108262.
893 Webster, Michael W., Ying-Hsin Chen, James A. W. Stowell, Najwa Alhusaini, Thomas Sweet, Brenton R.
894 Graveley, Jeff Coller, and Lori A. Passmore. 2018. "MRNA Deadenylation Is Coupled to Translation
895 Rates by the Differential Activities of Ccr4-Not Nucleases." *Molecular Cell* 70 (6): 1089-1100.e8.
896 Wu, Colin Chih-Chien, Amy Peterson, Boris Zinshteyn, Sergi Regot, and Rachel Green. 2020. "Ribosome
897 Collisions Trigger General Stress Responses to Regulate Cell Fate." *Cell* 182 (2): 404-416.e14.
898 Wu, Colin Chih-Chien, Boris Zinshteyn, Karen A. Wehner, and Rachel Green. 2019. "High-Resolution
899 Ribosome Profiling Defines Discrete Ribosome Elongation States and Translational Regulation
900 during Cellular Stress." *Molecular Cell* 73 (5): 959-970.e5.
901 Wu, Qiushuang, Santiago Gerardo Medina, Gopal Kushawah, Michelle Lynn DeVore, Luciana A. Castellano,
902 Jacqelyn M. Hand, Matthew Wright, and Ariel Alejandro Bazzini. 2019. "Translation Affects MRNA
903 Stability in a Codon-Dependent Manner in Human Cells." *ELife* 8 (April).
904 https://doi.org/10.7554/eLife.45396.

905 Xie, Zhuorui, Allison Bailey, Maxim V. Kuleshov, Daniel J. B. Clarke, John E. Evangelista, Sherry L. Jenkins,
906 Alexander Lachmann, et al. 2021. “Gene Set Knowledge Discovery with Enrichr.” *Current Protocols*
907 1 (3): e90.
908 Yan, Liewei L., Carrie L. Simms, Fionn McLoughlin, Richard D. Vierstra, and Hani S. Zaher. 2019. “Oxidation
909 and Alkylation Stresses Activate Ribosome-Quality Control.” *Nature Communications* 10 (1): 5611.
910 Yan, Liewei L., and Hani S. Zaher. 2019. “How Do Cells Cope with RNA Damage and Its Consequences?”
911 *The Journal of Biological Chemistry* 294 (41): 15158–71.
912

913 Data Availability

914 Ribo-seq data is available in the NCBI Gene Expression Omnibus (GEO)
915 (https://www.ncbi.nlm.nih.gov/geo/) database with the accession GSE189404. The mass spectrometry
916 proteomics data have been deposited to the ProteomeXchange Consortium via the PRIDE (Perez-Riverol
917 et al. 2019) partner repository with the dataset identifier PXD030076.

918 Acknowledgements

919 We thank Allen R. Buskirk, Niladri Sinha, and Nicolle Rosa Mercado for careful reading of the
920 manuscript and all Green lab members for helpful discussions throughout this study. High throughput
921 sequencing was performed at the Johns Hopkins Genetic Resources Core Facility (RRID: SCR_018669) and
922 the Johns Hopkins Single Cell and Transcriptomics Core. Mass spectrometry was performed by the Johns
923 Hopkins Mass Spectrometry Core.

924 Funding

925 Canadian Institutes of Health Research Foundation Grant FDN-159913

926 • Grant W. Brown

927 National Institutes of Health (R37GM059425)

928 • Rachel Green

National Institutes of Health (5T32GM135131-02)

- Juliette Lecomte